



1 Multi-model assessment of the deglacial climatic evolution at southern high latitudes

2 Takashi Obase¹, Laurie Menviel², Ayako Abe-Ouchi¹, Tristan Vadsaria¹³, Ruza Ivanovic⁴, Brooke Snoll⁴,
3 Sam Sherriff-Tadano⁴, Paul J. Valdes⁵, Lauren Gregoire⁴, Marie-Luise Kapsch⁶, Uwe Mikolajewicz⁶,
4 Nathaëlle Bouttes⁷, Didier Roche⁷, Fanny Lhardy⁷, Chengfei He⁸, Bette Otto-Bliesner⁹, Zhengyu Liu¹⁰,
5 Wing-Le Chan¹

6 ¹Atmosphere and Ocean Research Institute, The University of Tokyo, Kashiwa, Japan

7 ²Climate Change Research Center, The Australian Centre for Excellence in Antarctic Science, the
8 University of New South Wales, Sydney, Australia,

9 ³UiT The Arctic University of Norway, Tromsø, Norway

10 ⁴School of Earth & Environment, University of Leeds, Woodhouse Lane, Leeds, UK

11 ⁵School of Geographical Sciences, University of Bristol, University Road, Bristol, UK

12 ⁶Max Planck Institute for Meteorology, Hamburg, Germany

13 ⁷Laboratoire des Sciences du Climat et de l'Environnement/Institut Pierre-Simon Laplace, UMR CEA-
14 CNRS-UVSQ, Université Paris-Saclay, Gif-sur-Yvette, France

15 ⁸Rosenstiel School of Marine, Atmospheric, and Earth Science, University of Miami, Miami, FL, USA

16 ⁹Climate and Global Dynamics Laboratory, National Center for Atmospheric Research, Boulder, USA

17 ¹⁰Atmospheric Science Program, Department of Geography, Ohio State University, Columbus, USA

18 *Correspondence to:* Takashi Obase (obase@ori.u-tokyo.ac.jp)

19 **Abstract.** The quaternary climate is characterised by glacial-interglacial cycles, with the most recent
20 transition from the last glacial maximum to the present interglacial (the last deglaciation) occurring
21 between ~ 21 and 9 ka. While the deglacial warming at southern high latitudes is mostly in phase with
22 atmospheric CO₂ concentrations, some proxy records have suggested that the onset of the warming
23 occurred before the CO₂ increase. In addition, southern high latitudes exhibit a cooling event in the middle
24 of the deglaciation (15 - 13 ka) known as the Antarctic Cold Reversal (ACR). In this study, we analyse
25 transient simulations of the last deglaciation performed by six different climate models as part of the 4th
26 phase of the Paleoclimate Modelling Intercomparison Project (PMIP4) to understand the processes
27 driving southern high latitude surface temperature changes. While proxy records from West Antarctica
28 and the Pacific sector of the Southern Ocean suggest the presence of an early warming before 18 ka, only
29 half the models show a significant warming (~1°C or ~10% of the total deglacial warming). All models
30 simulate a major warming during Heinrich stadial 1 (HS1, 18 - 15 ka), greater than the early warming, in
31 response to the CO₂ increase. Moreover, simulations in which the AMOC weakens show a more



32 significant warming during HS1 as a result. During the ACR, simulations with an abrupt increase in the
33 AMOC exhibit a cooling in southern high latitudes, while those with a reduction in the AMOC in response
34 to rapid meltwater exhibit warming. We find that all climate models simulate a southern high latitude
35 cooling in response to an AMOC increase with a response timescale of several hundred years, suggesting
36 the model's sensitivity of AMOC to meltwater, and the meltwater forcing in the North Atlantic and
37 Southern Ocean affect southern high latitudes temperature changes. Thus, further work needs to be carried
38 out to understand the deglacial AMOC evolution with the uncertainties in meltwater history. Finally, we
39 do not find substantial changes in simulated Southern Hemisphere westerlies nor in the Southern Ocean
40 meridional circulation during deglaciation, suggesting the need to better understand the processes leading
41 to changes in southern high latitude atmospheric and oceanic circulation as well as the processes leading
42 to the deglacial atmospheric CO₂ increase.

43

44 **1. Introduction**

45 The recent Quaternary climate is characterised by glacial-interglacial cycles of about 100,000-
46 year periodicity (Lisiecki and Raymo, 2005; Jouzel et al., 2007). These glacial-interglacial cycles are
47 driven by insolation changes as external forcing and by feedbacks, including changes in atmospheric
48 greenhouse gas (GHG) concentrations and the waxing and waning of continental ice sheets, mainly in the
49 northern high latitudes (Abe-Ouchi et al., 2013). During the Last Glacial Maximum (LGM, ~21 ka; ka
50 indicates 1000 years before present), the continental ice sheets covered a significant area of the high
51 northern latitudes (Tarasov et al., 2012; Peltier et al., 2015), thus leading to a sea level fall of ~130 meters
52 compared to pre-industrial (Lambeck et al., 2014). The atmospheric CO₂ concentration was also ~100
53 ppm lower than the pre-industrial (Petit et al., 1999; Bereiter et al., 2015). These climatic boundary
54 conditions contributed to a colder climate during the LGM, with global mean surface air temperature
55 anomalies estimated to be 4.5 ± 0.9 °C lower than present-day (Annan et al., 2022). As the last deglaciation
56 (transition from the LGM to the early Holocene) represents one of the largest, most recent and well-
57 documented natural warming of the last million years, an understanding of the processes and feedbacks
58 during this time period can offer insight into our own modern changing world. Here, we focus on the
59 southern high latitudes, where deglacial warming began before their Northern Hemisphere (NH)



60 counterparts (Shakun et al., 2012), and which have been suggested to play a major role in driving the
61 increase in atmospheric CO₂ concentration. Although the timing of the onset of the deglacial warming at
62 southern high latitudes is poorly constrained, a compilation of Antarctic ice core records from East
63 Antarctica suggested that the deglacial Antarctic warming started at ~ 18 ka, in phase with the rise in
64 atmospheric CO₂ concentration (Parrenin et al., 2013). On the other hand, a record from the West
65 Antarctic Ice Sheet Divide ice core (WDC) suggests that the warming started at ~ 20 ka (Shakun et al.,
66 2012; WAIS project members, 2013). Moreover, an early onset of the deglacial warming (~21 ka) at mid-
67 southern latitudes has also been suggested based on SST and sea ice records from the Pacific sector of the
68 Southern Ocean (Moy et al., 2019; Sikes et al., 2019; Moros et al., 2021; Crosta et al., 2022).

69 Millennial-scale climate events are superimposed on the deglacial warming. At the beginning of
70 the deglaciation, during Heinrich stadial 1 (HS1, ~18 to 14.7 ka, following Ivanovic et al., 2016),
71 Greenland and the North Atlantic region remained cold (Buizert et al., 2014, Martrat et al., 2007), while
72 significant warming occurred at southern high latitudes (WAIS project members, 2010). This period was
73 associated with a weakening of the Atlantic Meridional Ocean Circulation (AMOC), evidenced by Pa/Th
74 in marine sediments (McManus et al., 2004; Ng et al., 2018). During the subsequent Bølling-Allerød (BA,
75 ~14.7 to 12.8 ka) period, Greenland surface air temperatures rose by more than 10°C in just a few decades
76 (Stephensen et al., 2008; Buizert et al., 2014), and the AMOC strengthened significantly (Severinghaus
77 & Brook, 1999; McManus et al., 2004; Roberts et al., 2010; Ng et al., 2018). A cooling event at southern
78 high latitudes, known as the Antarctic Cold Reversal (ACR), was identified between ~15 and 13 ka
79 (Jouzel et al. 2007; Pedro et al., 2016), concurrent with the BA. The Younger-Dryas (YD, 12.8 to 11.7
80 ka) followed the BA, and was characterised by a drastic cooling in Greenland and the North Atlantic.
81 While the processes leading to the YD are still debated (Renssen et al., 2015), it has been suggested that
82 the YD can be attributed to a weakening of the AMOC (McManus et al., 2004), caused by a rerouting of
83 freshwater into the Arctic that was then transported toward the deep-water formation sites of the subpolar
84 North Atlantic by coastal boundary currents (Condrón and Winsor, 2012; Kapsch et al., 2022). Climate
85 model simulations with marine proxy constraints support the variations in the AMOC during the last
86 deglaciation (Pöppelmeier et al., 2023).



87 An AMOC weakening causes a warming in the South Atlantic as the meridional oceanic heat
88 transport to the North Atlantic is weakened (Stocker & Johnsen, 2003; Stouffer et al., 2006). This
89 warming can then be propagated into the Southern Ocean and Antarctica (Pedro et al., 2018). The
90 contrasting temperature changes between Greenland and the southern high latitudes can also be found
91 during abrupt events of the last ice age known as Dansgaard–Oeschger cycles (Dansgaard 1993; NGRIP
92 project members, 2004; WAIS Divide project members, 2015), which have led to the notion of a bipolar
93 seesaw (Stocker and Johnsen 2003; Capron et al., 2010). Alongside these events, the atmospheric CO₂
94 increase throughout the deglaciation occurred in steps, suggesting a link to millennial-scale climate events
95 (Marcott et al., 2014) and changes in Southern Ocean circulation contributing to degassing of oceanic
96 carbon (Anderson et al., 2009, Menviel et al., 2018).

97 Transient climate simulations provide a suitable framework for assessing the processes leading to
98 deglacial climate changes. Early transient simulations that were conducted with transient orbital forcing,
99 GHGs and ice sheets suggested that an increase in spring insolation in the southern high latitudes was
100 responsible for the onset of warming (Timmermann et al., 2009), and that deglacial warming of the
101 Southern Ocean appeared as early as ~20 to 18 ka in association with sea ice retreat (Roche et al., 2011).
102 Transient simulations that also included freshwater input into the North Atlantic highlighted the AMOC
103 impact on climate change (Liu et al., 2009; He et al., 2011). Menviel et al. (2011) further assessed whether
104 the ACR was a response to the strong AMOC increase at the end of HS1 or whether it was caused by
105 enhanced meltwater input from the Antarctic ice sheet. These simulations were designed to simulate
106 AMOC changes in agreement with estimates from proxy records, and therefore the magnitude, location,
107 and timing of the implemented meltwater fluxes were idealised. In contrast, experiments forced with
108 meltwater fluxes consistent with ice sheet reconstructions based on sea-level constraints often simulate
109 millennial-scale AMOC changes in disagreement with accepted interpretations of climate and ocean
110 records. Some experiments simulate an AMOC weakening at the time of the BA because of significant
111 mass loss of NH ice sheets (Bethke et al., 2012; Ivanovic et al., 2018a; Kapsch et al., 2022; Bouttes et al.,
112 2023) or do not simulate any abrupt climate events (Gregoire et al., 2012). With an idealised scenario that
113 follows the evolution of NH ice sheets more closely (except for the 14 ka meltwater pulse), the MIROC
114 climate model shows that it is possible to simulate an abrupt AMOC strengthening with the presence of



115 continuous freshwater in the North Atlantic because of gradual warming (Obase and Abe-Ouchi, 2019).
116 These studies indicate that different models have different sensitivities in terms of the AMOC response
117 to forcing and, therefore, it is useful to analyse multi-model results for a robust understanding of the
118 climatic processes.

119 To facilitate further examination of the mechanisms driving deglacial climate change, a protocol
120 for carrying out transient simulations of the last deglaciation was proposed as part of the fourth phase of
121 the Paleoclimate Modeling Intercomparison Project (PMIP4) (Ivanovic et al., 2016). The protocol of
122 PMIP4 deglaciation summarised climate forcing (ice core based atmospheric GHGs and reconstructed
123 ice sheets) for climate model experiments. The protocol is designed to be flexible in that the use of some
124 boundary conditions is determined by each modelling group, which allows an explorations of different
125 climate scenarios. The multi-model assessment of the last deglaciation performed here provides an
126 opportunity to investigate the mechanism of past climate changes and to evaluate the uncertainties from
127 the models' sensitivity to the forcings.

128 Some boundary conditions for climate models, including GHG and Antarctic ice sheet (prescribed
129 in PMIP4 protocol), result from climate change at the southern high latitudes. Proxy records and
130 modelling studies indicate that physical and biogeochemical changes in the Southern Ocean may have
131 significantly contributed to ocean carbon uptake during glacial periods, and that early deglacial changes
132 in the Southern Ocean could have provided a major contribution to the atmospheric CO₂ increase observed
133 during HS1 (Sigman et al., 2010, Skinner et al., 2010, Martinez-Garcia et al., 2011, Bouttes et al., 2012,
134 Meniel et al., 2016, Meniel et al., 2018, Gottschalk et al., 2019). Subsurface warming on the Antarctic
135 shelf contributes to the mass loss of Antarctic ice sheets through enhanced melting of ice shelves, and
136 retreat of grounding lines (Golledge et al., 2014; Lowry et al., 2019). In addition, climate conditions at
137 southern high latitudes can impact the formation of the Antarctic Bottom Water (AABW) and the shoaling
138 of AMOC (Sherriff-Tadano et al., 2023). Hence investigating the climate evolution at southern high
139 latitudes may give an insight into critical climate system feedback during the last deglaciation.

140 Here, we analyse the deglacial climatic evolution (21–11 ka) at southern high latitudes as
141 simulated in six PMIP4 transient experiments, and compare the results with paleo-proxy records. We
142 mainly focus on the Antarctic surface air temperature (SAT) and Southern Ocean sea surface temperature



143 (SST) changes. As there is a substantial difference between the AMOCs in the simulations, we utilise
144 statistical or simple models to assess the impact of changes in atmospheric CO₂ and AMOC on Southern
145 Ocean SST. We analyse the evolution of the AABW, Southern Ocean westerlies and subsurface ocean
146 temperature in the Southern Ocean to discuss critical climate system feedbacks occurring at southern high
147 latitudes.

148

149 **2 Methods**

150 **2-1 Climate models and experiments used in this study**

151 We use the PMIP4 transient simulations of the last deglaciation performed with six atmosphere-
152 ocean coupled climate models (Table 1). These simulations are initialised with LGM conditions. The
153 Equilibrium Climate Sensitivity (ECS, defined by global mean SAT changes in response to doubling CO₂
154 from the pre-industrial) of each model ranges from 2.0 to 3.9 °C, and the global mean surface air
155 temperature (SAT) anomaly for the LGM is 3.5 to 7.3 °C (Table 1). Table 2 summarises the experimental
156 design of each model simulation and their reference articles. While some of the modelling groups
157 performed two or more sensitivity experiments with different model parameters or boundary conditions
158 (e.g., different freshwater forcing (FWF) scenarios or ice sheets), for this study we have selected one
159 representative simulation from each climate model. Fig. 1 summarises the time evolution of the climate
160 forcings, i.e. insolation, atmospheric GHGs, and continental ice sheets used in the simulations. Both
161 reconstructions (ICE-6G_C VM5a, henceforth ‘ICE-6G_C’; and ‘GLAC-1D’) have larger Antarctic ice
162 sheet volume at the LGM, with a ~ 10 m sea-level equivalent volume change at the LGM, relative to
163 present-day. Both suggest ~ 100 m of elevation change since the LGM at EPICA Dome C (EDC, 123°E,
164 75°S), while WAIS Divide (WDC, 112°W, 79.5°S) differs by 300 meters between the two datasets (Fig.
165 1d).

166 Fig. 2a summarises the total amount of FWF in the NH in six simulations. The FWF schemes can
167 be classified into two groups: [a] FWF adjusted to reproduce large-scale AMOC variability (iTRACE,
168 LOVECLIM, MIROC) and [b] FWF consistent with the reconstructed ice volume changes (HadCM3,
169 MPI-ESM, iLOVECLIM) based on ICE-6G_C or GLAC-1D (Fig. 2a, black lines). Notably, during HS1,
170 iTRACE and LOVECLIM have significant FWF (~ 0.2 Sv), while other simulations apply FWF of less



171 than 0.1 Sv. In LOVECLIM and MIROC, the meltwater flux was uniformly applied to the North Atlantic,
172 while other models use the location of the melting NH ice-sheet and associated runoff to apply a spatially
173 varying FWF (Table 2). ICE-6G_C (HadCM3, MPI-ESM, iLOVECLIM) leads to a meltwater input of
174 about 0.1 Sv to the Southern Ocean at 11.5–11 ka. iTRACE and LOVECLIM also applied freshwater flux
175 to the Southern Ocean to simulate the ACR (iTRACE: up to 0.2Sv during 14.4–13.9 ka, LOVECLIM:
176 fixed at 0.09Sv during 14.67–14.1 ka).

177 In section 3.3, we conduct further analysis to examine the processes driving Southern Ocean SST
178 using a multilinear regression (MLR) model and a thermal bipolar seesaw model adapted from Stocker
179 and Johnsen (2003).

180

181 **2-2: Simple models to disentangle CO₂ and AMOC**

182 **2-2-1: Multilinear Regression model**

183 We use a MLR model to regress changes in SST onto CO₂ and AMOC variations:

$$184 \quad SST = \alpha * CO_2 + \beta * AMOC + \gamma, \quad (1)$$

185 where *SST* (Southern Ocean SST, averaged over 55–40°S), and *AMOC* (defined as the maximum
186 meridional overturning streamfunction in the North Atlantic, at depths below 500 m and 20–60°N) are
187 output from the climate models, and *CO₂* is the forcing used in each simulation. The AMOC in the analysis
188 is normalised with respect to the maximum and minimum values in each model. The CO₂ is also
189 normalised with respect to the total change between 21 and 11 ka (~83 ppm). The MLR analysis is applied
190 to the time-varying areally-averaged Southern Ocean SST values and time-varying 2-D fields of the
191 Southern Ocean SST, respectively. Every 100-year mean SST, AMOC, and CO₂ from 20 to 11 ka are
192 used as the input for this analysis, so each dataset has 90 time-slices. One note is that we do not consider
193 insolation nor other forcings, because the insolation forcing and CO₂ are not independent; both gradually
194 change during the last deglaciation (Fig. 1).

195 **2-2-2: Thermal bipolar seesaw model**

196 As the MLR model does not consider transient climate response, we construct a thermal bipolar
197 seesaw model following Stocker and Johnsen (2003). The original thermal bipolar seesaw model is based
198 on an energy balance between the North and South Atlantic Oceans. We add the effect of CO₂ on



199 temperature, which was not considered in the original model. The thermal bipolar seesaw model in this
200 study solves the temporal evolution of SST using the following equations:

201
$$\frac{dSST}{dt} = \frac{SSTeq - SST(t)}{\tau} \quad (2)$$

202
$$SSTeq = \alpha * CO_2(t) + \beta * m(t) \quad (3)$$

203 where $SSTeq$ is an equilibrium temperature (change since the LGM) expected from the CO_2 and state of
204 the AMOC at time t . $SST(t)$ is the SST change since LGM at time t , and τ is the characteristic timescale
205 of the bipolar seesaw. $CO_2(t)$ is the CO_2 concentration at time t , and is normalised with maximum and
206 minimum values as in the MLR model. The term $m(t)$ represents the modes of the AMOC (strong or
207 weak) from the climate model outputs. Based on AMOC values in each model, we assume $m(t)=0$ if the
208 AMOC is greater than 14 Sv, and $m(t)=1$ if the AMOC is smaller than 14 Sv.

209 Every 100-year mean AMOC and CO_2 value from 20 to 11 ka are used as the input, as the time
210 step is set to 100 years. The thermal bipolar model is initialised with $SST=0$. We investigate the best
211 combinations of parameters (α , β , τ) based on systematic sensitivity experiments, with combinations of
212 parameters shown in Table 3 (9610 set of parameters for each model). We find the best combinations of
213 parameters based on a minimum root mean square error estimator applied to simulated and actual SST
214 changes in each model.

215

216 3. Results

217 3-1: AMOC

218 As AMOC variations can impact southern high latitude climate, we summarise here the transient
219 evolution of the AMOC in the different simulations. As detailed below, the AMOC evolution is
220 substantially affected by the FWF schemes. All simulations except for MIROC display a strong (>20 Sv)
221 AMOC at the LGM (Fig. 2b). This is in line with the majority of PMIP4 simulations that display stronger
222 AMOC at the LGM than during Pre-Industrial (PI; Kageyama et al., 2021), although it is not consistent
223 with LGM reconstructions from multiple marine tracers (Lynch-Stieglitz et al., 2007; Bohm et al., 2015,
224 Menviel et al., 2016). During the period corresponding to HS1, the AMOC stays weak in MIROC and
225 significantly declines in the iTRACE and LOVECLIM simulations, as meltwater is added into the North
226 Atlantic. On the other hand, in the other simulations, there is only a slight reduction in AMOC (~ 1 Sv) as



227 the meltwater input into the North Atlantic stays below 0.05 Sv. At the BA (~14.7 ka), three models
228 exhibit an abrupt change from weak to strong AMOC, triggered by a rapid reduction in FWF (iTRACE
229 and LOVECLIM) or as a response to the gradual background warming (MIROC). These simulations
230 featuring an AMOC strengthening broadly agree with marine proxy records (Fig. 2b black line). On the
231 other hand, the other three simulations (HadCM3, MPI-ESM, iLOVECLIM) display an AMOC
232 weakening due to a significant increase in FWF originating from the ice sheet collapse associated with
233 Meltwater Pulse 1a (Deschamps et al., 2012). During the Younger-Dryas (12.8–11.7 ka), iTRACE,
234 LOVECLIM, and MIROC simulate an AMOC decline, corresponding to an increase in FWF or an
235 oscillatory nature of the AMOC in MIROC (Kuniyoshi et al., 2022). HadCM3 simulates a gradual AMOC
236 reduction, while MPI-ESM exhibits multi-centennial AMOC variability. At 11 ka, the AMOC strength
237 returns to a strong mode except for iLOVECLIM, which stays weak after the BA.

238 **3-2 SST and SAT**

239 Fig. 3 summarises the simulated Antarctic SAT and Southern Ocean SST changes since the LGM
240 in all the simulations (LGM is defined as 21 ka in most models, with some exceptions because of
241 differences in the timing of initialisation; 20.6 ka for LOVECLIM, 20.0 ka for iTRACE). The SAT at
242 WDC and EDC are compared with the ice core based reconstructions from Parrenin et al. (2013) and
243 Buizert et al., (2021).

244 **3-2-1: 21–18ka (onset of warming)**

245 This period corresponds to mostly stable atmospheric CO₂, with an increase in spring to summer
246 insolation at southern high latitudes driven primarily by obliquity change (Fig. 1a). Three models
247 (MIROC, HadCM3, MPI-ESM) exhibit a gradual ~1°C warming between 21 and 18 ka at both WDC and
248 EDC (Fig. 3c). This simulated EDC warming is comparable with EDC ice core estimates (Parrenin et al.,
249 2013). However, the magnitude of warming suggested from WDC (~2°C warming between 19.5–19 ka,
250 Shakun et al., 2012) is not simulated by any of the models (Fig. 4a). On the other hand, a slight cooling
251 is simulated at WDC in iTRACE and at EDC in LOVECLIM, with the latter exhibiting little change (Fig.
252 4a).



253 Significant SAT warming in MIROC, HadCM3 and MPI-ESM occurs at the same time as a 0.5–
254 1.0°C SST warming in the Southern Ocean north of the sea ice edge, and a gradual reduction in Southern
255 Ocean sea ice area (Figs. 3f and 4).

256 **3-2-2: 18–14.7ka (HS1)**

257 This period corresponds to an increase in CO₂ from 190 to 230 ppm. Reconstructions from the
258 WDC and EDC suggest a 4–8°C warming (Fig. 3c–d). All models exhibit a larger warming during this
259 period than between 21 and 18 ka. iTRACE simulates the largest warming (+6–8°C), closely following
260 the estimates from ice core data. The sharp increase in temperature in iTRACE starts at ~18 ka,
261 corresponding to a period of major reduction in AMOC strength (Fig. 3b). The warming in MPI-ESM
262 follows iTRACE with a 5°C warming, despite a minor reduction in AMOC strength. The HadCM3
263 exhibits ~4°C warming at WDC and ~2°C warming at EDC, while the other models simulate a 2–4°C
264 warming at EDC and WDC (Fig. 3c–d). iTRACE exhibits the most significant Southern Ocean SST
265 warming at 5 °C and LOVECLIM exhibits a sharp Southern Ocean SST increase, ~3°C, in response to an
266 AMOC reduction at ~17 ka. The other models' Southern Ocean SST increase by 1–2 °C (Fig. 3e).
267 Southern Ocean sea ice area exhibits the same trends as the Southern Ocean SST, with iTRACE
268 simulating the largest sea ice area reduction of up to 40% compared to the LGM (Fig. 4b).

269 **3-2-3: 14.7–13ka (BA)**

270 At 14.7 ka the abrupt and large warming of the BA is recorded in Greenland, while a gradual 2°C
271 cooling (ACR) is recorded at WDC and EDC between 14.7 and 13 ka. Three models (iTRACE, MIROC,
272 LOVECLIM) simulate an abrupt AMOC increase at the BA onset, and a concomitant cooling at southern
273 high latitudes: ~1-2 °C Antarctic SAT and Southern Ocean SST decrease. iTRACE and LOVECLIM
274 exhibit a sharp cooling in Southern Ocean SST and SAT in the early phase of the BA, probably enhanced
275 by the meltwater flux into the Southern Ocean (Menviel et al., 2011). In contrast, the three other models
276 (HadCM3, MPI-ESM, iLOVECLIM) exhibit a warming in the early phase of the BA, corresponding to
277 an AMOC weakening. Subsequently, HadCM3 and MPI-ESM exhibit a gradual cooling over the
278 Antarctic and Southern Ocean as the AMOC strengthens in the later part of the BA (~13.5 ka).
279 iLOVECLIM displays a rapid warming at 13.5 ka, followed by a cooling despite the AMOC being weak



280 throughout this period, which is explained by abrupt surface albedo changes caused by the evolving land-
281 sea mask in the Antarctic region (Bouttes et al., 2023).

282 **3-2-4: 13–11ka (YD and Holocene onset) and total deglacial warming**

283 This period corresponds to the YD, during which an AMOC weakening has been suggested
284 (McManus et al., 2004, Ng et al., 2018). Both EDC and WDC reconstructions show a 2–4°C warming
285 between 13 and 12 ka. During that time, iTRACE, MIROC, and LOVECLIM simulate an AMOC
286 weakening as well as a southern high latitude warming. iTRACE simulates a ~3–4°C increase in Southern
287 Ocean SST, while LOVECLIM and MIROC simulate a 1°C warming. MPI-ESM exhibits multi-
288 centennial variability associated with variations in AMOC strength. MPI-ESM and iLOVECLIM exhibit
289 sharp cooling in Southern Ocean SST and SAT starting at ~11.5 ka, enhanced by the meltwater flux into
290 the Southern Ocean (Kapsch et al., 2022).

291 The total deglacial (21–11 ka) warming is 10 °C in WDC, while the EDC estimates range from 5
292 to 10 °C (Parrenin et al., 2013; Buizert et al., 2021). Across the simulations, a 2 to 10 °C warming is
293 simulated over Antarctica. Only one model (MPI-ESM) simulates a larger warming at EDC than at WDC,
294 while three models suggest a larger temperature change at WDC (iTRACE, HadCM3, LOVECLIM), and
295 two models show a similar warming at both sites (MIROC, iLOVECLIM). In line with the WDC and the
296 upper range of EDC estimates, iTRACE and MPI-ESM display a 8–10 °C total warming over Antarctica.
297 The Southern Ocean sea ice edge retreats poleward by 10° latitude in most models. A SST increase of up
298 to 6 °C is simulated in this area in iTRACE, LOVECLIM, HadCM3, and MPI-ESM, while a ~4 °C SST
299 increase is simulated in MIROC and iLOVECLIM (Fig. 5).

300 The different magnitudes of warming between models could be explained by the range of
301 temperature changes between LGM and PI, as the mean SAT and SST changes are different by a factor
302 of two (Table 1). To reduce this model difference, Antarctic SAT are normalised by the temperature
303 anomaly between LGM and PI. When normalised, iTRACE still has the largest warming (Fig. 6a),
304 MIROC and LOVECLIM display the second and third-largest warming for HS1. One common point in
305 these three models is the weak AMOC in HS1 (Fig. 6b left). Even if the total amount of global warming
306 is small, the weakening of AMOC in HS1 with MIROC and LOVECLIM contributes to HS1 warming as
307 in iTRACE. In contrast, the other three models (HadCM3, MPI-ESM, and iLOVECLIM) exhibit mostly



308 strong AMOC during HS1, and the normalised HS1 warming were smaller (Fig. 6 right panels). The
309 normalised Antarctic SAT change at 11 ka varies between 0.3–0.8 with respect to the total temperature
310 change between LGM and PI, indicating that some warming also occurred after the onset of the Holocene.
311 This marks a main difference between the simulations and proxy data, in that the temperature at 11 ka is
312 comparable to the pre-industrial values based on ice core reconstructions (Parrenin et al., 2013; Buizert
313 et al., 2021).

314 **3-3: SST – CO₂ – AMOC relationship analysis**

315 The simulated AMOC time series display large differences across simulations derived from
316 different FWF schemes, which complicates the quantification of the relative importance of CO₂ forcing
317 and AMOC changes in driving southern high latitude temperature changes in each model. To overcome
318 this, we examine the Southern Ocean SST trajectory against CO₂ forcing, and AMOC strength (Fig. 7).
319 Fig. 7 clearly shows that the deglacial increase in atmospheric CO₂ has significant impacts on the Southern
320 Ocean SST because the temperature trajectory is mostly proportional to CO₂ changes unless there are
321 significant AMOC changes. Temperature changes associated with changes in AMOC are superimposed
322 on Southern Ocean SSTs, in that an AMOC weakening or strengthening (blue or red circles) tends to
323 induce warming or cooling, respectively. Even though the actual time series of AMOC in each model are
324 very different, this result suggests that southern high latitude temperature changes can be decomposed
325 into the effects of CO₂ and AMOC. The relative importance of CO₂ and AMOC are quantified in the
326 following subsections.

327

328 **3-4: Results of MLR model**

329 The results of the MLR model indicate that the CO₂ coefficients range from 1.0 to 6.5°C for the
330 total deglacial CO₂ changes (Table 4). All models have a negative coefficient of AMOC (–0.3 to –2.4°C),
331 indicating a Southern Ocean SST increase for an AMOC weakening. The results suggest that an AMOC
332 shutdown during HS1 has the potential to increase temperature as CO₂ increases (which is able to explain
333 about half of the total deglacial changes during HS1).

334 The regression against Southern Ocean 2-D SST fields indicates that the CO₂ coefficient is mostly
335 positive over the Southern Ocean, ranging from ~0.5 °C in the Antarctic zone where sea ice is present



336 until 11 ka, to 2–6 °C in the Southern Ocean north of the LGM winter sea ice edge (Fig. 8). The sensitivity
337 to the AMOC is mostly negative in the Southern Ocean, and areas of high sensitivity overlap with those
338 of CO₂, suggesting sea ice modulates the areas sensitive to both CO₂ and AMOC changes.

339 **3-5: Results of bipolar seesaw model**

340 Table 5 summarises the results of the bipolar seesaw model. All models have positive CO₂
341 coefficients (2.0–6.0°C) and negative AMOC coefficients (–0.5 to –2.9°C), as in the MLR models. The
342 time series simulated by the bipolar seesaw model are compared with actual SST changes and with MLR
343 models in Fig. 9. The bipolar seesaw model succeeds in reproducing a gradual SST decrease as a result
344 of an AMOC strengthening (e.g. gradual cooling in iTRACE and MIROC, 15–13 ka). This gradual
345 cooling was not represented by the MLR model, which exhibits an immediate SST response to AMOC
346 changes. The response time ranges from 100–700 years, with most models ranging from 500–700 years
347 with the exception of LOVECLIM and iLOVECLIM (Table 5).

348 We note that a sharp cooling associated with freshwater in the Antarctic Ocean was not
349 represented because both models, MLR and bipolar seesaw, do not consider meltwater in the Southern
350 hemisphere (~14.5 ka of iTRACE and LOVECLIM, ~11.5 ka of MPI-ESM and iLOVECLIM)

352 **3-6: Other Southern Ocean climate variables**

353 We analyse AABW transport (minimum global meridional overturning streamfunction, at depths
354 below 3000 m and 60°S–30°S) as an indicator of Southern Ocean meridional circulation, and 850 hPa
355 zonal mean winds over the Southern Ocean (zonal mean winds averaged over 65°S–40°S). We focus on
356 the onset of deglaciation (21–18 ka) and the initial significant increase in CO₂ (~HS1, 18–15 ka). The
357 AABW (Fig. 10b) at the LGM ranges from 10 to 30 Sv among the six models and stays relatively constant
358 between 21 and 18 ka. In the subsequent period (18–15 ka), iTRACE exhibits a significant decline in the
359 AABW, in phase with Southern Ocean SST changes (Fig. 10d). LOVECLIM and MPI-ESM exhibit a
360 gradual decline in AABW (~5 Sv), while three other models (MIROC, HadCM3, iLOVECLIM) exhibit
361 a small reduction or a stable AABW. The zonal winds over the Southern Ocean do not change
362 significantly between 21 and 18 ka, apart from MIROC and MPI-ESM, which exhibit a slight weakening
363 (Fig. 10c). Between 18 and 15 ka, the zonal winds continue to decline in MIROC and MPI-ESM, and also



364 start to decline in iTRACE and LOVECLIM. Little changes in zonal winds are simulated in iLOVECLIM,
365 while HadCM3 exhibits a ~10% strengthening.

366 Subsurface ocean temperatures south of 60°S at depths of around 500 m (Fig. 10e) exhibit an
367 increase during HS1 in 4 of the 6 simulations, with the largest warming (1.2 °C and 0.8 °C) simulated by
368 the two simulations which exhibited the largest SST increase (iTRACE and MPI-ESM). During the ACR
369 (15–13 ka), iTRACE and MIROC exhibit a gradual sub-surface temperature decrease while HadCM3 and
370 MPI-ESM exhibit a continuous warming, as per the SST changes in the respective models. iLOVECLIM
371 and LOVECLIM exhibit small changes (<0.5°C) in the total sub-surface temperature. Abrupt subsurface
372 warming in iTRACE (~14 ka) and LOVECLIM (14.8–14.2 ka) coincide with Southern Ocean SST
373 reduction, suggesting that this results from enhanced Southern Ocean stratification as a response to
374 Southern Ocean meltwater input (Menviel et al., 2011; Lowry et al., 2018).

375 **4. Discussion**

376 **4-1: Onset of deglacial warming**

377 The climate forcing in the early deglaciation primarily comes from insolation due to obliquity and
378 precession changes (Fig. 1a), which leads to an increase in spring to summer insolation south of 60 °S
379 (Fig. S1). Ice core data suggest that the onset of deglacial warming at WDC was earlier than the increase
380 in CO₂, and this early deglacial warming has been suggested to result from an AMOC reduction (Shakun
381 et al., 2012) or local insolation changes (WAIS project members, 2013). Not all models show such
382 warming and when a warming is simulated, it is smaller than estimated from proxy records. Three models
383 (MIROC, HadCM3, MPI-ESM) exhibit a small but significant warming (~ 0.5°C) between 21 and 18 ka
384 (Fig. 4a) in both West and East Antarctica, as well as in Southern Ocean SST, primarily in the Pacific
385 sector (Fig. 4b) as suggested by proxy records (Moy et al., 2019; Sikes et al., 2019; Moros et al., 2021).
386 Although the amplitude of the early warming in these models is comparable to a previous modelling study
387 (Timmermann et al., 2009), the other models show a slight cooling (iTRACE and LOVECLIM) or little
388 change (iLOVECLIM).

389 The first explanation for the differences in the simulated temperature change between 21 and 18
390 ka is the contrast in LGM climate states, and in particular, the extent of Southern Ocean sea ice. MIROC,



391 HadCM3 and MPI-ESM have less LGM summer sea ice than other climate models, and the winter sea
392 ice does not reach as far north: the northern margin of winter sea ice extent is located at $\sim 60^\circ\text{S}$ in the
393 Pacific sector, while it is at $50\text{--}55^\circ\text{S}$ in the other models (Fig. 4b bold lines). We note that these results
394 for sea ice extent are within the range of reconstructions, as most recent proxy records combined with
395 PMIP climate models estimated austral winter and summer sea ice extent to be around $60\text{--}55^\circ\text{S}$ and 65°S ,
396 respectively (Lhardy et al., 2022; Green et al., 2022). The smaller sea ice extent at the LGM may allow
397 the Southern Ocean to absorb increased incoming shortwave radiation during austral spring to summer,
398 and induce significant warming with sea ice retreat (Timmermann et al., 2009; Roche et al., 2011). If the
399 LGM Southern Ocean sea ice extent is extensive, the increase in insolation primarily south of 60°S (Fig.
400 S1) does not warm the Southern Ocean as much because of high sea ice albedo. The second explanation
401 is the difference in the FWF. The three simulations that display an early deglacial warming include a FWF
402 ($\sim 0.02\text{ Sv}$) in the North Atlantic based on ICE-6G_C (Fig. 2a). An early ice sheet discharge from the
403 Fennoscandian ice sheet (Touccane et al., 2010) could have weakened the AMOC and contributed to the
404 Southern Ocean warming.

405 Another model-data difference is the different early warming rates between West and East
406 Antarctica. The data from WDC suggests there was significant warming in West Antarctica, while a less
407 significant change in East Antarctica is suggested by EDC. In contrast, the models simulate similar
408 warming rates in both West and East Antarctica (Fig. 4a), suggesting the models may underestimate the
409 spatial heterogeneity in West and East Antarctic warming. This might be attributed to the Antarctic ice
410 sheet history prescribed in the experiments, where both ICE-6G_C and GLAC-1D have minor surface
411 elevation changes at WDC in the early deglaciation (Fig. 1d). Buizert et al. (2021) used the MIROC and
412 HadCM3 models and showed that the uncertainty in Antarctic ice sheet height affects the difference
413 between LGM and PI temperatures because changes in surface elevation affect SAT ($\sim 1^\circ\text{C}$ per 100 m).
414 This might suggest that the lower surface elevations at WDC, related to the ice sheet terminus retreat
415 between 20–15 ka in the Amundsen Sea (Bentley et al. 2014), may have contributed to the early deglacial
416 warming primarily in West Antarctica.

417 Uncertainty in the Antarctic ice sheet could also explain some model-data differences during the
418 early Holocene, where simulations indicate more warming occurs after the onset of the Holocene (Fig. 6).



419 This is different from ice core data (Fig. 4) and global mean ocean temperature (including deep-sea
420 temperature) estimated from noble gases in ice cores, which suggests that temperatures reached Holocene
421 levels at the end of YD (Bereiter et al., 2018). The higher surface elevation of the Antarctic ice sheet at
422 11 ka compared to the present-day in the experimental design (Fig. 1e) may contribute to the simulated
423 Holocene warming.

424 **4-2: Rate of temperature changes**

425 HS1 (~18–14.7 ka) exhibits significant warming in all models because of the CO₂ increase, with
426 the total warming being dependent on the sensitivity of each model to CO₂ and to AMOC changes.
427 iTRACE simulates the largest warming, 6–8°C, in both WDC and EDC, which is the closest to the
428 warming rate from ice-core data among the six models. Estimates from the MLR and bipolar seesaw
429 models indicate that both the increase in CO₂ during HS1 (~ 40 ppm) and the reduction in AMOC
430 contributed to this warming. iTRACE notably exhibits the largest global mean SAT changes at the LGM
431 (7.3 °C, compared to the six-model mean of 5.3 °C). However, the ECS of iTRACE (3.6 °C) is not the
432 highest among the six models; MIROC4m has the highest ECS (Table 1). We examine the relationship
433 between ECS and the LGM global mean SAT changes using multi-model PMIP3 and PMIP4 simulations
434 (Fig. S4). We find a weak negative correlation (–0.06) between the ECS and global mean LGM SAT
435 changes, and the SAT anomalies in the individual climate models can vary by about a factor of two even
436 with the same ECS. A substantial asymmetry between warm and cold climates has been identified in
437 previous studies because of the presence of continental ice sheets, ocean dynamics, and cloud feedback
438 (Yoshimori et al., 2009; Zhu and Poulsen, 2021). Hence, a good understanding of the forcing and climate
439 system feedback of the LGM climate is critical for evaluating the rate of warming during the last
440 deglaciation.

441 The sensitivity to AMOC ranges from 0.5–2.9 °C, based on the analysis using the thermal bipolar
442 seesaw model (Table 5). A multi-model study comparing freshwater hosing experiments of 11 climate
443 models (including LOVECLIM, MIROC, and HadCM3 used in this study) under LGM climate shows
444 that a majority of models exhibit warming in the Southern Ocean (Kageyama et al., 2013). However, the
445 simulation length in their study is less than 420 years, as opposed to the estimated timescale in this study



446 (~500–700 years), suggesting the need for longer simulations to estimate the extent of the climate
447 response at southern high latitudes.

448 The MLR and thermal bipolar seesaw models in this study may have a limited ability in
449 disentangling the effects of CO₂ and AMOC or in considering non-linear responses. For example, the
450 AMOC sensitivity of the LOVECLIM model seems low compared to the 1.5 °C Southern Ocean SST
451 increase found in the simulation of Heinrich stadial 4, in which the atmospheric CO₂ concentration was
452 kept constant (Margari et al. 2020, Fig. S2). In addition, a MIROC simulation with a larger freshwater
453 (0.1 Sv) during HS1 than in the standard deglaciation experiment exhibits a 0.5 °C higher Southern Ocean
454 SST with a 3 Sv weaker AMOC (Fig. S3), indicating that the Southern warming in response to AMOC
455 strength is nonlinear. Finally, the coefficients of CO₂ and AMOC are not necessarily constant in time,
456 and other climate forcings derived from insolation and continental ice sheets can impact temperature
457 changes. Despite these limitations, these analyses can provide estimates of each model's deglacial
458 sensitivity to CO₂ forcing and AMOC.

459 As shown here, the deglacial AMOC variations are quite different amongst the simulations. Only
460 those which display an AMOC increase at the end of HS1 can capture a cooling trend corresponding to
461 the ACR as suggested by ice-core data (iTRACE, LOVECLIM, MIROC). In comparison to previous
462 transient simulations of the last deglaciation, the representation of the duration of the ACR has improved,
463 as it was previously simulated as too short (Lowry et al., 2018). On the other hand, simulations that are
464 forced with a large NH meltwater pulse consistent with ice sheet reconstructions do not simulate an ACR
465 (Ivanovic et al., 2016; 2018; Kapsch et al., 2022; Bouttes et al., 2023). Regarding the BA, investigating
466 the impacts of changing boundary conditions, typically those of ice sheets, GHGs and insolation, is
467 necessary to reduce the gap between the climate responses and ice sheet reconstructions. Southern FWF
468 can enhance the ACR, as found in iTRACE (~14.2 ka) and LOVECLIM (~14.7 ka), with a sharp cooling
469 in Southern Ocean SST and Antarctic SAT primarily in WDC. This is caused by the intensified
470 stratification in the Southern Ocean (Menviel et al., 2010; 2011), which induces significant warming in
471 the subsurface and contributes to further mass loss from Antarctic ice sheets (Golledge et al., 2014). As
472 ice core data does not exhibit such sharp cooling events as compared to climate model simulations (Fig.
473 3), this may provide some constraints on the extent and duration of FWF from the Antarctic ice sheet.



474

475 **4-3: Implications for climate system changes in southern high latitudes**

476 Reconstructions have suggested that changes in Southern Ocean circulation, probably driven by
477 wind changes, were important for the modulation of Southern Ocean CO₂ outgassing during the
478 deglaciation. In particular, marine sediment cores from the sub-Antarctic zone suggest an enhanced opal
479 flux during HS1, which could reflect increased upwelling in the Southern Ocean due to changes in
480 Southern Hemispheric westerlies (SHW) (Anderson et al., 2009). This is consistent with decreasing deep
481 and intermediate-depth Southern Ocean ventilation ages (Skinner et al., 2010, Burke et al., 2011),
482 increasing intermediate-depth pH in the Southern Ocean during HS1 (Rae et al., 2018), and a compilation
483 of Southern Ocean δ¹⁸O records indicating a poleward shift of the SHW across the deglaciation (Gray et
484 al., 2023). Stronger or poleward-shifted SHW and/or enhanced AABW formation during HS1 would
485 indeed enhance Southern Ocean CO₂ outgassing and lead to an atmospheric CO₂ increase comparable to
486 that from ice core estimates (Menviel et al., 2014; Menviel et al., 2018). In contrast, most models show
487 very little change or a gradual weakening in the SHW across the deglaciation, and there is little latitudinal
488 migration of the SHW. Only the HadCM3 model displays a SHW strengthening. However, additional
489 studies should look in more details into potential changes in the location of the SHW in these simulations,
490 as well as regional changes in SHW strength and their relation to other climatic variables (Rojas et al.,
491 2009; Sime et al., 2013). In addition, no model exhibits an increase in AABW, which could contribute to
492 the upwelling of carbon-rich water mass in the deep ocean and CO₂ outgassing from the Southern Ocean.
493 Instead, the deglaciation may have contributed to the long-term weakening in AABW by warming the
494 Southern Ocean, enhancing sea ice melt, and decreasing surface salinity (Marson et al., 2016). While it
495 has been suggested that larger Southern Ocean sea ice extent would lead to an atmospheric CO₂ decrease
496 at the LGM (Marzocchi et al., 2020, Stein et al., 2020), few models simulate significant changes in oceanic
497 CO₂ due to a Southern Ocean sea ice change (Gottschalk et al., 2019). These physical changes still need
498 to be reconciled with processes put forward to explain the deglacial atmospheric CO₂ changes by running
499 coupled climate-carbon simulations.

500 Finally, we also find that changes in subsurface ocean temperature in the Southern Ocean, one of
501 the critical factors impacting the retreat of the Antarctic ice sheet, display significant differences across



502 the simulations. This could be related to different ECS or FWF in the Southern Ocean, and should also
503 be investigated in future studies to quantify uncertainties in subsurface ocean temperature changes.
504 Model-dependent subsurface ocean temperature change is one source of uncertainty in projecting future
505 Antarctic ice sheet mass loss (Serrousi et al., 2020). In contrast to the present simulations of the last
506 deglaciation, which prescribe the Antarctic ice sheet history, climate variability occurring during the
507 deglaciation can impact the Antarctic ice sheet, which can act as feedback to Southern Ocean climate via
508 meltwater input from the Antarctic ice sheet (Menviel et al., 2010; Golledge et al., 2014; Clark et al.,
509 2020). Hence, further coupled climate and ice sheet modelling studies are needed to improve our
510 understanding of climatological and glaciological processes and to evaluate model performance under a
511 warming climate and rising sea levels (Gomez et al., 2020).

512 **5. Conclusion**

513 In our multi-model analysis of transient deglacial experiments, most models simulate the onset of
514 the deglacial warming at southern high latitudes between 18 and 17 ka, in phase with the atmospheric
515 CO₂ increase. The early warming simulated in some models could be related to the smaller LGM sea ice
516 extent, which may affect the sensitivity to insolation change, or to a slight reduction in the AMOC in
517 response to small freshwater input from NH ice sheets. The models do not exhibit significant differences
518 in the warming rates between West and East Antarctica, contrary to what is suggested by ice core records.
519 The most rapid warming occurs between 18 and 15 ka in response to increased CO₂ concentration, with
520 the rate of warming being related to the climate sensitivity of each model. The reduction in the AMOC
521 during HS1 associated with increased freshwater flux in the North Atlantic as imposed in some models
522 further contributes to the warming. The simulations further suggest that an abrupt AMOC increase at the
523 end of HS1 is necessary to simulate the southern high latitude cooling corresponding to the ACR. The
524 amplitude and duration of the cooling is different between the models because of the different North
525 Atlantic freshwater scenarios, and the different amplitudes and timescales of bipolar climate responses in
526 each model. The simulations do not exhibit significant changes in winds over the Southern Ocean or
527 meridional circulation in the Southern Ocean, which could contribute to enhanced CO₂ outgassing from
528 the Southern Ocean. This indicates the necessity for future climate system modelling studies to quantify
529 the sequence of climate changes and atmospheric CO₂ increase during the last deglaciation.



530

531 **Acknowledgements:**

532 TO, AAO, TV and WLC acknowledge funding from JSPS Kakenhi 17H06104, 17H06323, and
533 JPJSBP120213203. We acknowledge discussions at PAGES-QUIGS T5–T0 workshops, supported by
534 INQUA Terminations Five to Zero (T5–T0) Working Group (Project #2004). LM acknowledges funding
535 from Australian Research Council (ARC) grants FT180100606 and SR200100008. UM and MK
536 acknowledge funding by the German Federal Ministry of Education and Research as a Research for
537 Sustainability Initiative through the PalMod project (grant nos. 01LP1915C, and 01LP1917B). The MLR
538 analysis used scikit-learn library of Python 3.7. The figures were created using Generic Mapping Tool
539 (GMT version 4 and 6).

540

541 **Data availability:**

542 All model data supporting our findings will be archived at Zenodo. Original model data is upon
543 request for authors from each modelling group.

544 **Code availability:**

545 The bipolar seesaw model and the MLR model used in this study can be shared upon request.

546 **Author contribution:**

547 TO, LM, and AAO conceived the study. TO, LM, TV, BS analysed the data. TO, LM, AAO, TV,
548 RI, and BS wrote the manuscript with input from all co-authors.

549 **Competing interests:**

550 Laurie Menviel is a member of the editorial board of Climate of the Past, but otherwise all authors
551 declare that they have no conflict of interest.

552 **References:**

Name	Climate model name	ECS [K]	Global mean LGM SAT anomaly [K]	References
iTRACE	iCESM1.3	3.6	7.3	Tierney et al., (2020)
LOVECLIM	LOVECLIM	2.8	4.2	McDougall et al., (2020)



MIROC	MIROC4m	3.9	4.5	Chan and Abe-Ouchi, (2020)
HadCM3	HadCM3B	2.7	6.1	Kageyama et al., (2021)
MPI-ESM	MPI-ESM-CR P2		6.1	
iLOVECLIM	iLOVECLIM	2.0	3.5	

553 **Table 1:** Summary of climate models analysed in this study. Note that the ECS for MPI-ESM (model
 554 version MPI-ESM-CR P2) has not been calculated.

555

Name	Freshwater scheme	GHGs	Ice sheets	References for deglaciation experiments
iTRACE	TraCE-like	PMIP4	ICE-6G_C	He et al., 2019; 2021
LOVECLIM	TraCE-like	Kohler et al., 2017	ICE-5G	Menviel et al., 2011
MIROC	ICE-6G_C with adjustment	PMIP4	ICE-5G (LGM fix)	Obase and Abe-Ouchi 2019; Obase et al., 2021
HadCM3	ICE-6G_C	PMIP4	Ice-6G_C	Ivanovic et al., 2018; Snoll et al., 2022
MPI-ESM	ICE-6G_C	Kohler et al., 2017	Ice-6G_c	Kapsch et al., 2022
iLOVECLIM	ICE-6G_C	PMIP4	Ice-6G_c	Bouttes et al., 2023

556 **Table 2:** Summary of the experimental design used in the transient deglacial simulations.

557

Parameter [unit]	Range
CO ₂ coefficient α [K/83 ppm]	1.0–7.0, every 0.2
AMOC coefficient β [K/(normalised AMOC)]	0.0–3.0, every 0.1
Response timescale τ [year]	100–1000, every 100

558 **Table 3:** Parameter ranges in the thermal bipolar seesaw model.

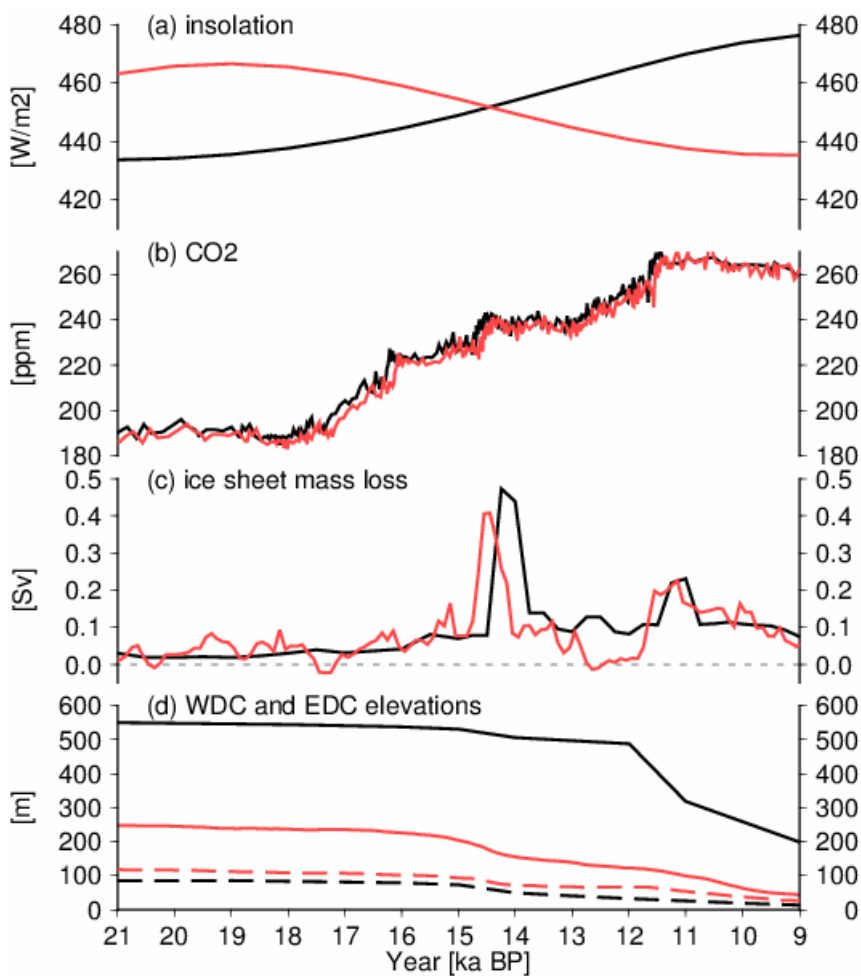


	CO ₂ coefficient [K/83 ppm]	AMOC coefficient [K/(normalised AMOC)]	Coefficient of Determination
iTRACE	6.5	-2.4	0.90
LOVECLIM	4.1	-0.4	0.91
MIROC	1.4	-0.5	0.81
HadCM3	3.3	-1.4	0.95
MPI-ESM	3.1	-1.2	0.90
iLOVECLIM	1.0	-1.4	0.56

559 **Table 4:** Results of the MLR model for Southern Ocean SST.

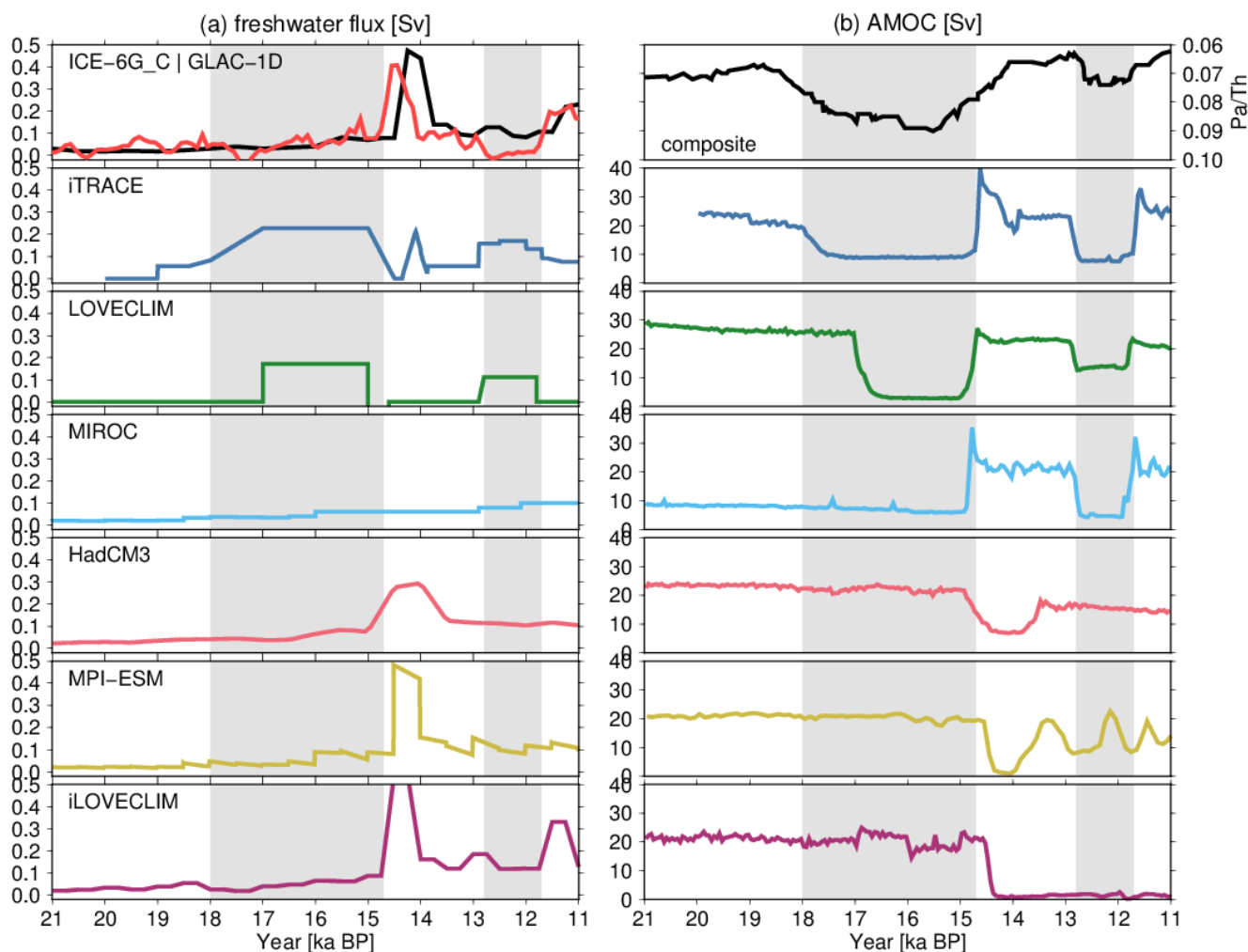
	CO ₂ coefficient [K/83 ppm]	AMOC coefficient [K/(normalised AMOC)]	Response timescale [year]
iTRACE	6.0	-2.9	500
LOVECLIM	4.4	-0.6	300
MIROC	2.4	-0.9	600
HadCM3	4.8	-1.3	700
MPI-ESM	3.4	-1.4	500
iLOVECLIM	2.0	-0.8	100

560 **Table 5:** Results of the bipolar seesaw model for Southern Ocean SST



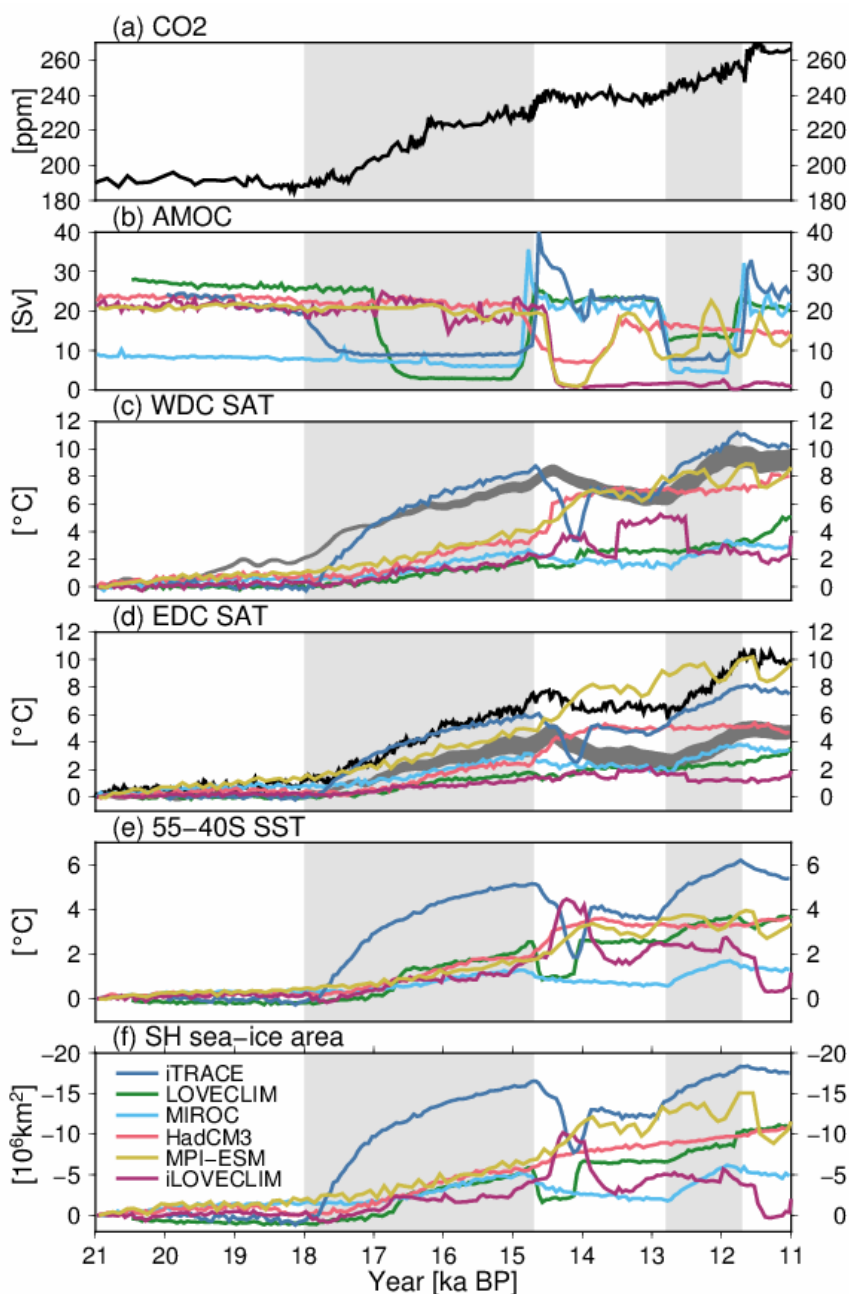
561

562 **Figure 1:** Forcing of the last deglaciation. (a) Insolation. Black: 65°N July, red: 65°S January based on
563 Berger (1978), (b) CO₂. Black: Bereiter et al., (2015), red: Kohler et al., (2017), (c) FWF in the NH from
564 ICE-6G_C (black lines) and GLAC-1D (red lines), (d-e) Elevation change at WDC (bold lines) and EDC
565 (dashed lines) from ICE-6G_C and GLAC-1D.



566

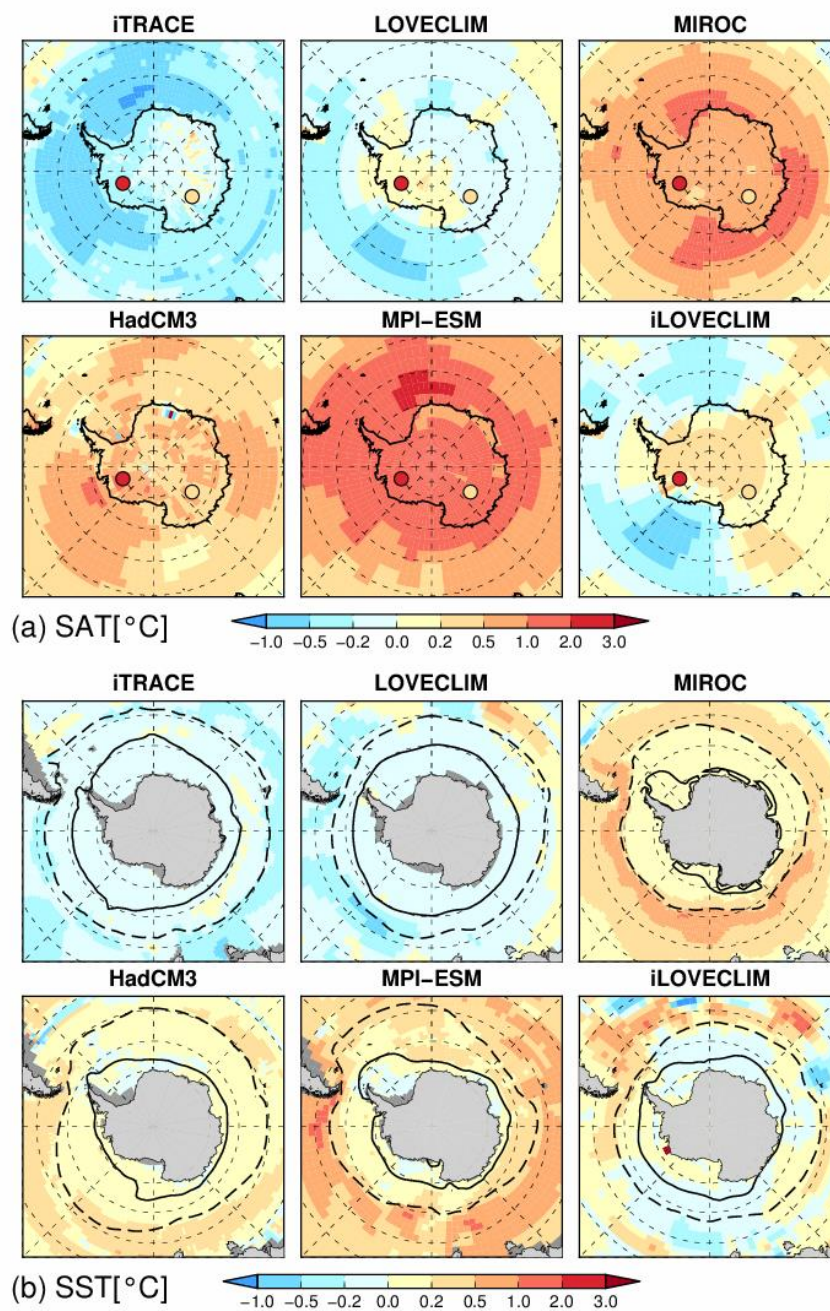
567 **Figure 2:** (a) Freshwater forcing (total value in the NH) and (b) simulated time series of AMOC. The top
568 panels indicate the freshwater flux from ice sheet reconstructions (black indicates ICE-6G_C and red
569 indicates GLAC-1D) and composite $^{231}\text{Pa}/^{230}\text{Th}$ in the North Atlantic, retrieved from Ng et al., (2018).
570 The grey shading indicates HS1 (18–14.7ka) and the YD (12.8–11.7ka), respectively, and the period in
571 between corresponds to the BA (14.7–12.8 ka).



572

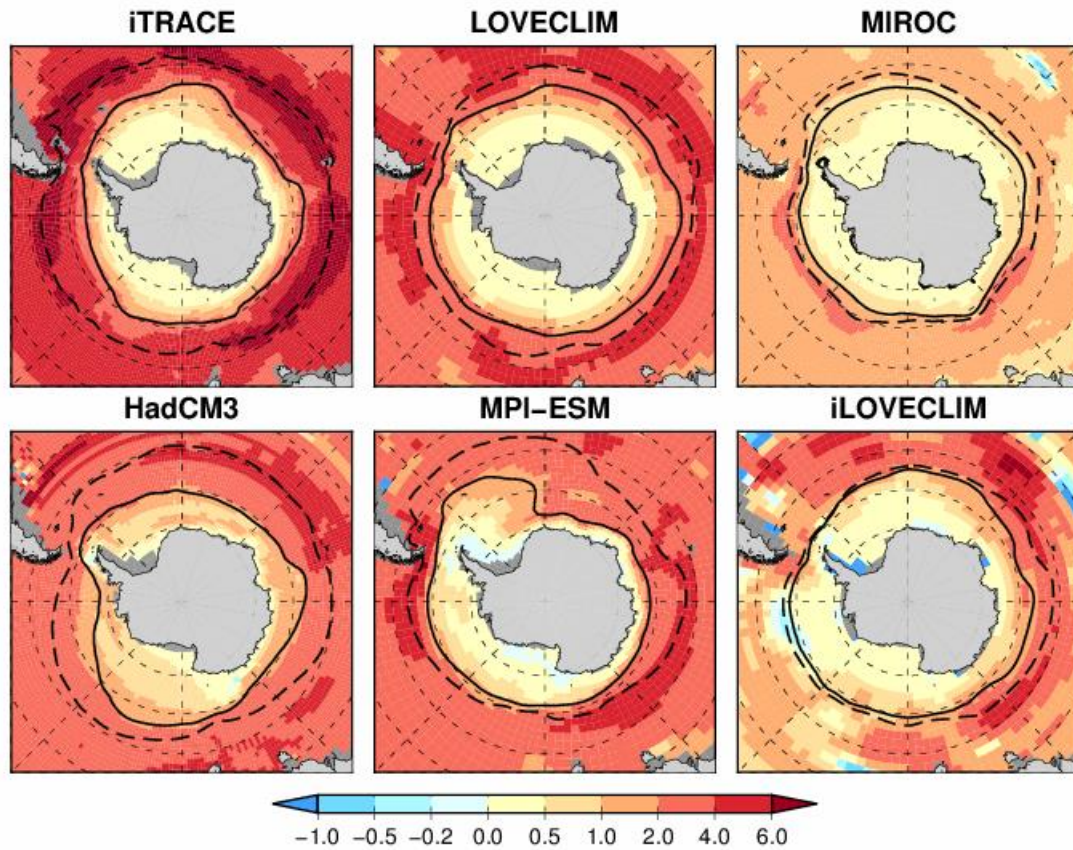
573 **Figure 3:** Time series of (a) atmospheric CO₂ (Bereiter et al., 2015) and (b) simulated AMOC, (c–d) SAT
574 at WDC and EDC, (e) Southern Ocean SST, (f) Southern Ocean sea ice area in the transient simulations.
575 The SAT, SST and sea ice area indicate changes since the LGM. The grey lines in (c–d) represent
576 reconstructions from Buizert et al., (2013), and the black line in (d) represents reconstructions from
577 Parrenin et al., (2013).

578



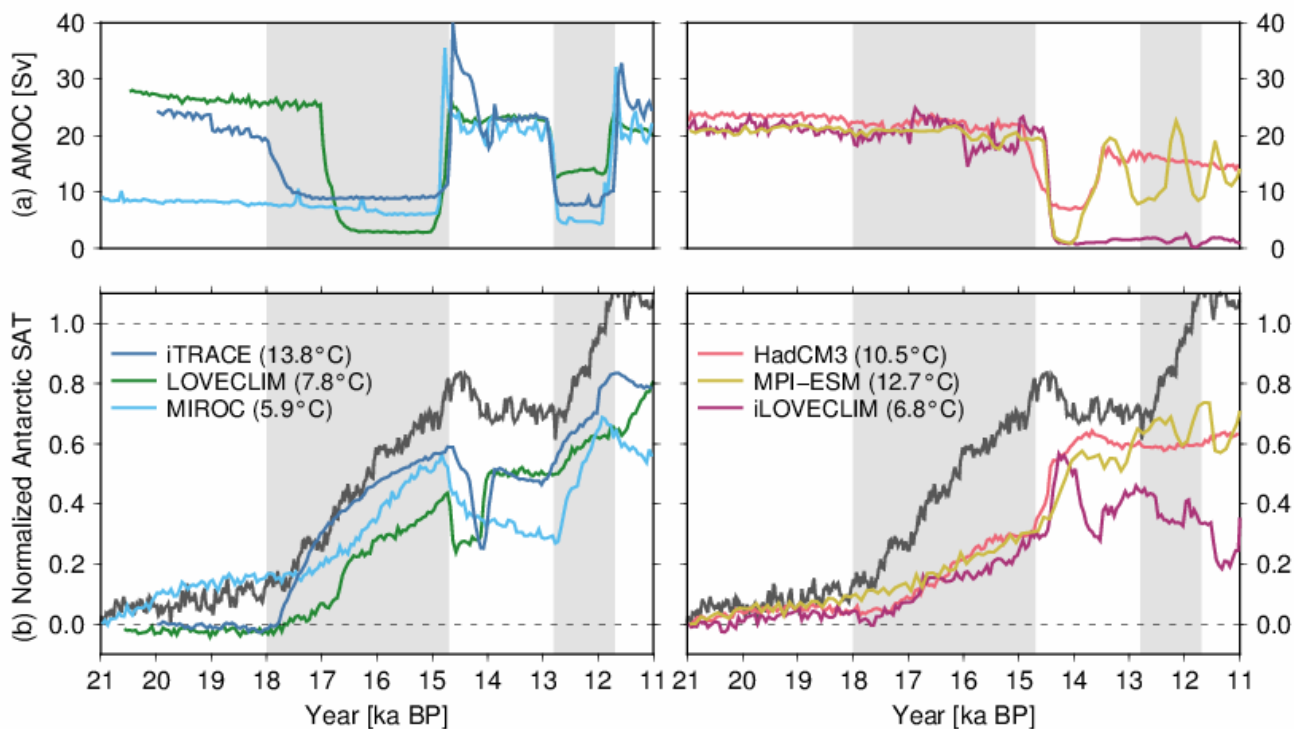
579

580 **Figure 4:** (a) SAT and (b) SST anomalies at 18 ka compared to the LGM. The coloured circles in (a)
581 represent 18 ka-LGM warming based on ice core data (Parrenin et al., 2013), and the bold and dashed
582 lines in (b) represent LGM austral summer and winter sea ice extent (85 and 15% annual-mean sea ice
583 concentration).



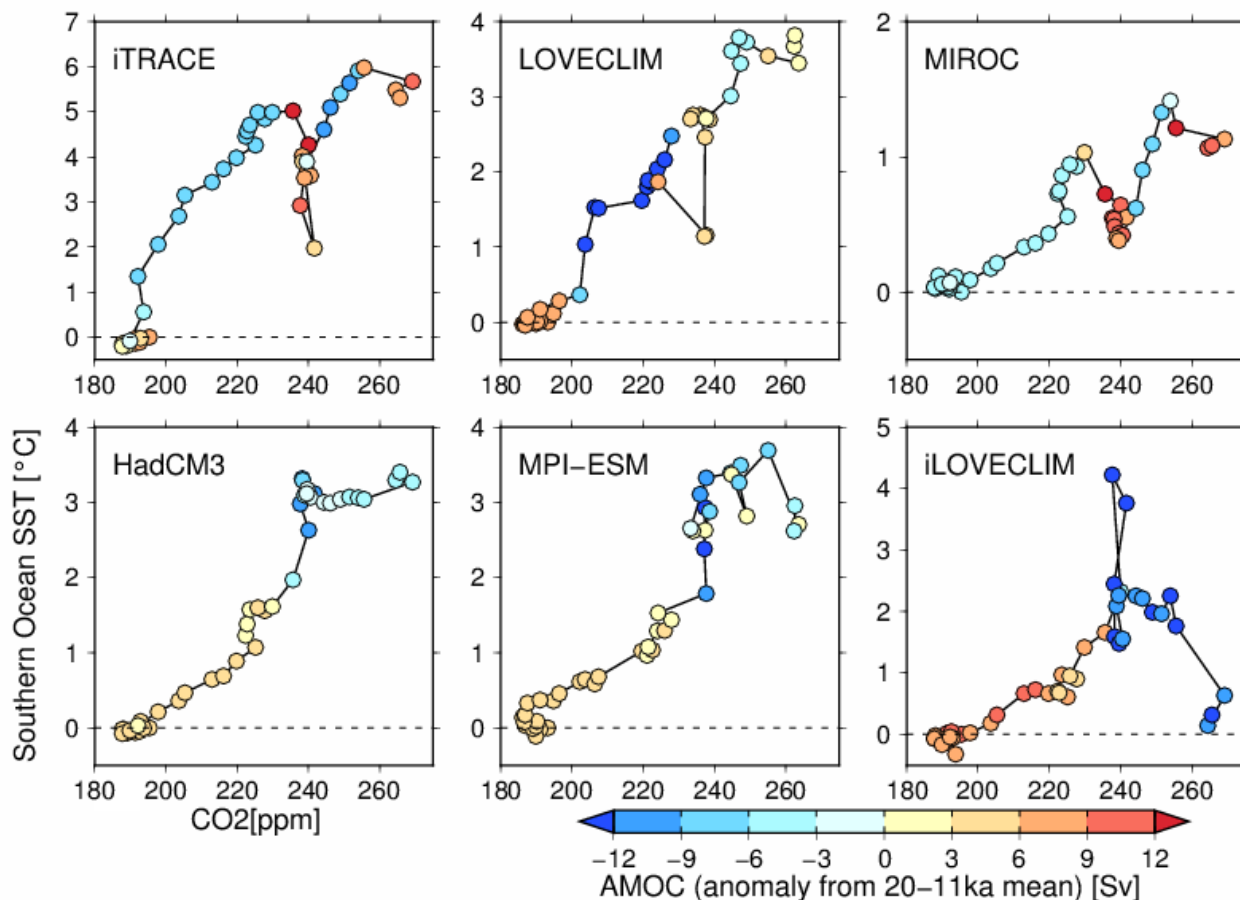
584

585 **Figure 5:** SST anomalies at 11 ka compared to the LGM. The bold and dashed lines indicate LGM and
586 11 ka sea ice extent (15% sea ice concentration), respectively.



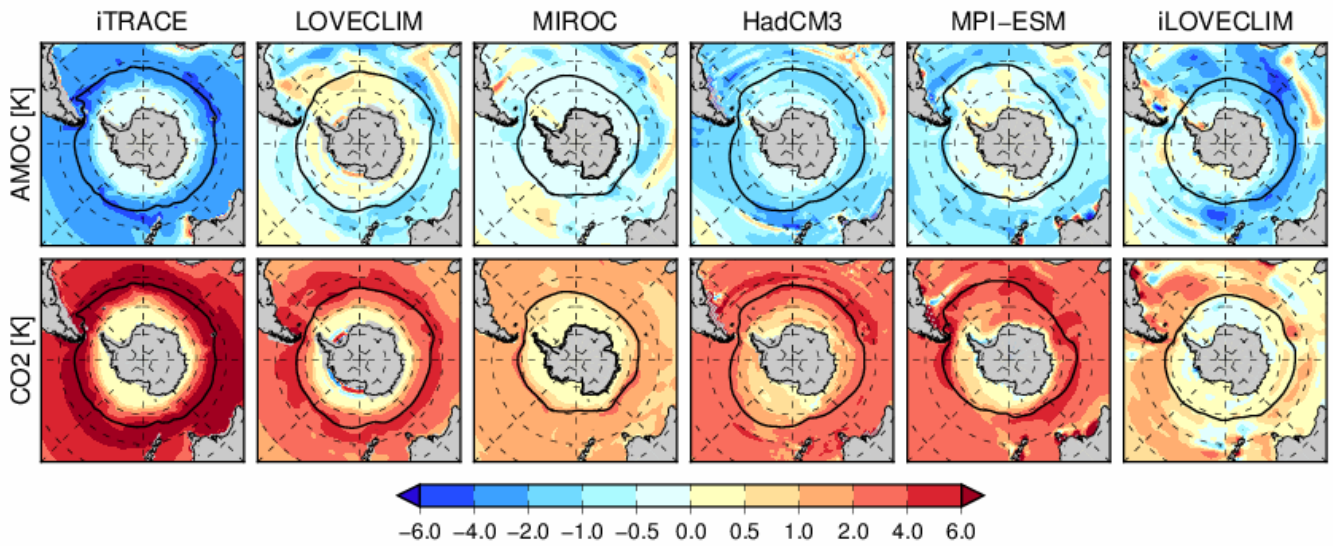
587

588 **Figure 6:** AMOC, and Antarctic SAT normalised with respect to the difference between PI and LGM.
589 The actual PI and LGM differences are indicated in parentheses. The left panels show three simulations
590 with weak AMOC during HS1, and the right ones show strong AMOC during HS1. The grey line in (b)
591 is the normalised Antarctic SAT from EDC based on Parrenin et al., 2013.



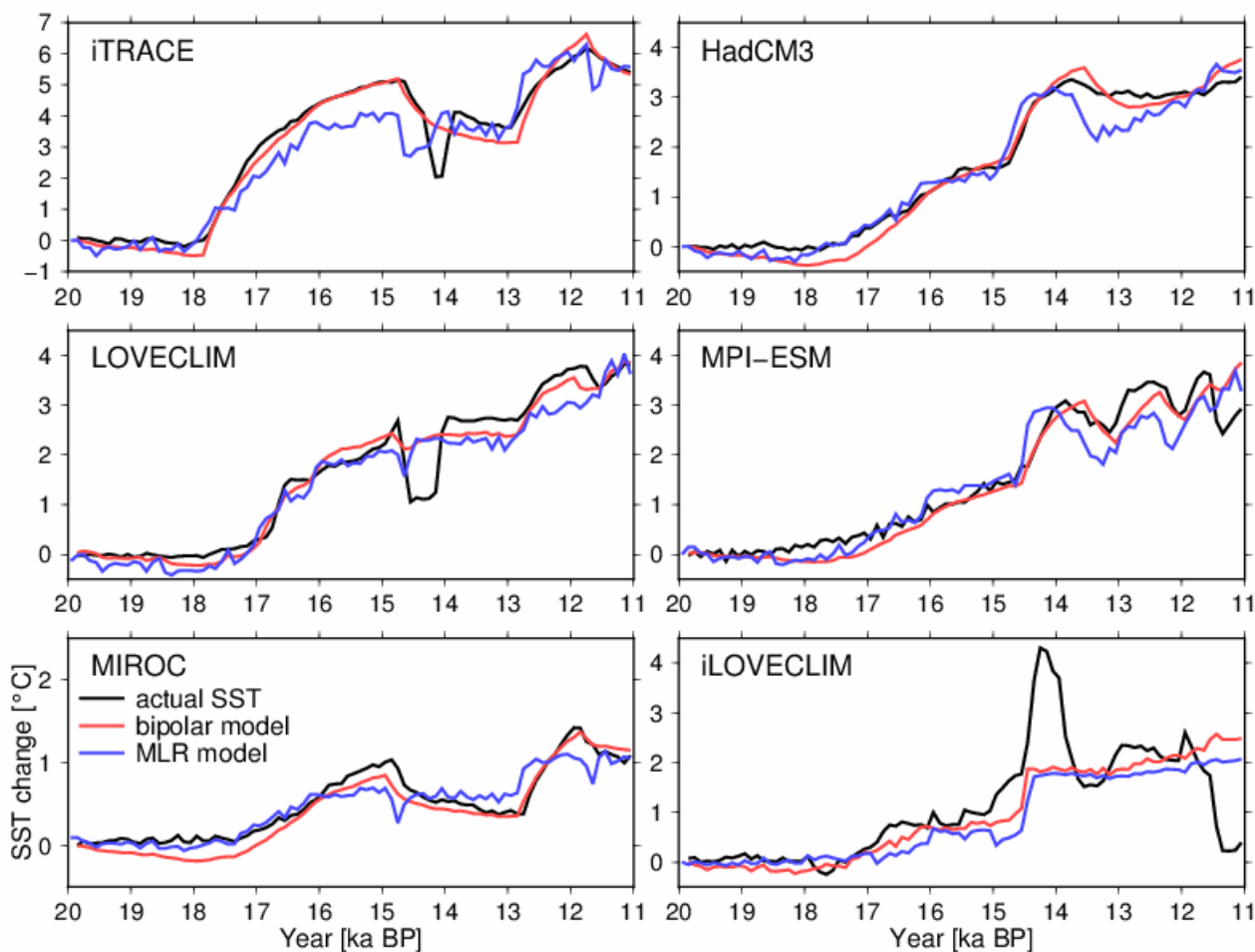
592

593 **Figure 7:** Relationship between Southern Ocean SST (vertical axis, change since LGM), CO₂ (horizontal
594 axis) and AMOC strength anomaly from the mean strength between 20–11 ka (colours). The trajectory
595 of the deglacial CO₂ forcing (CO₂), simulated SST changes and AMOC are plotted with circles at 200-
596 year intervals. Note that the vertical axes are different between models to represent the total deglacial
597 warming.



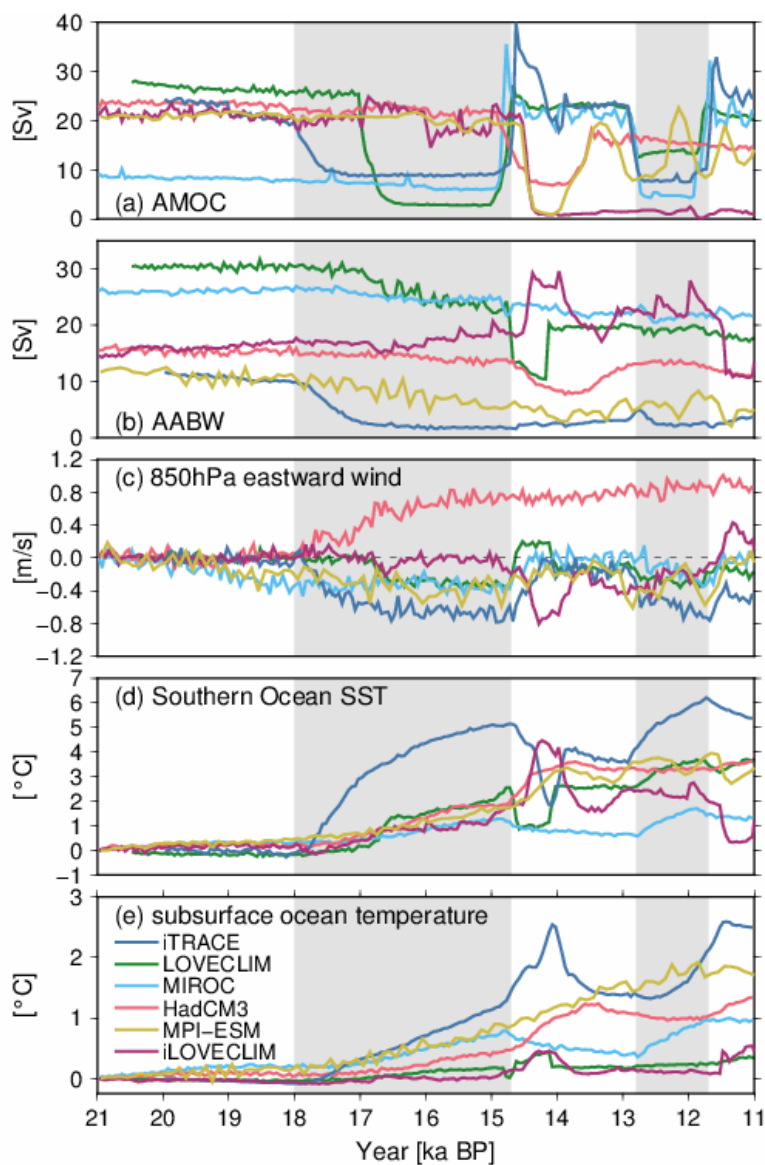
598

599 **Figure 8:** Results of the MLR model for 2-D SST maps. Top: AMOC coefficients. Bottom: CO₂
600 coefficients. The black lines represent LGM sea ice edges.



601

602 **Figure 9:** Results of the MLR model and bipolar seesaw model for Southern Ocean SST. The black lines
603 represent the actual SST change (anomaly from 20 ka). The blue and red lines represent the results of
604 MLR and bipolar seesaw models, respectively.



605

606 **Figure 10:** Time series of simulated (a) AMOC, (b) AABW, (c) 850hPa winds over the Southern Ocean
607 (65–40°S), (d) Southern Ocean SST, and (e) subsurface ocean temperature south of 60°S (at depths 400–
608 666 m).

609

610 **References**



- 611 1. Abe-Ouchi, A., Saito, F., Kawamura, K., Raymo, M. E., Okuno, J., Takahashi, K., and Blatter, H.:
612 Insolation-driven 100,000-year glacial cycles and hysteresis of ice-sheet volume. *Nature* 500, 190–
613 193, doi: 10.1038/nature12374, 2013
- 614 2. Anderson, B. E., & Burckle, L. H.: Rise in Atmospheric CO₂. *Science*, 323 (March), 1443–1448,
615 2009
- 616 3. Annan, J. D., Hargreaves, J. C., and Mauritsen, T.: A new global surface temperature reconstruction
617 for the Last Glacial Maximum, *Clim. Past*, 18, 1883–1896, <https://doi.org/10.5194/cp-18-1883-2022>,
618 2022.
- 619 4. Bentley, M. J., Ocofaigh, C., Anderson, J. B., Conway, H., Davies, B., Graham, A. G. C., Hillenbrand,
620 C. D., Hodgson, D. A., Jamieson, S. S. R., Larter, R. D., Mackintosh, A., Smith, J. A., Verleyen, E.,
621 Ackert, R. P., Bart, P. J., Berg, S., Brunstein, D., Canals, M., Colhoun, E. A., Crosta, X., Dickens,
622 W. A., Domack, E., Dowdeswell, J. A., Dunbar, R., Ehrmann, W., Evans, J., Favier, V., Fink, D.,
623 Fogwill, C. J., Glasser, N. F., Gohl, K., Golledge, N. R., Goodwin, I., Gore, D. B., Greenwood, S. L.,
624 Hall, B. L., Hall, K., Hedding, D. W., Hein, A. S., Hocking, E. P., Jakobsson, M., Johnson, J. S.,
625 Jomelli, V., Jones, R. S., Klages, J. P., Kristoffersen, Y., Kuhn, G., Leventer, A., Licht, K., Lilly, K.,
626 Lindow, J., Livingstone, S. J., Massé, G., McGlone, M. S., McKay, R. M., Melles, M., Miura, H.,
627 Mulvaney, R., Nel, W., Nitsche, F. O., O'Brien, P. E., Post, A. L., Roberts, S. J., Saunders, K. M.,
628 Selkirk, P. M., Simms, A. R., Spiegel, C., Stollendorf, T. D., Sugden, D. E., van der Putten, N., van
629 Ommen, T., Verfaillie, D., Vyverman, W., Wagner, B., White, D. A., Witus, A. E., and Zwartz, D.:
630 A community-based geological reconstruction of Antarctic Ice Sheet deglaciation since the Last
631 Glacial Maximum, *Quaternary Sci. Rev.*, 100, 1–9, <https://doi.org/10.1016/j.quascirev.2014.06.025>,
632 2014.
- 633 5. Berger, A.: Long-Term Variations of Daily Insolation and Quaternary Climatic Changes, *J. Atmos.*
634 *Sci.*, 35, 2362–2367, doi:10.1175/1520-0469(1978)035<2362:LTVODI>2.0.CO;2, 1978.
- 635 6. Bereiter, B., Eggleston, S., Schmitt, J., Nehrbass-Ahles, C., Stocker, T. F., Fischer, H., Kipfstuhl, S.,
636 and Chappellaz, J.: Revision of the EPICA Dome C CO₂ record from 800 to 600 kyr before present,
637 *Geophys. Res. Lett.*, 42, 542–549, 10.1002/2014GL061957, 2015.



- 638 7. Bereiter, B., Shackleton, S., Baggenstos, D., Kawamura, K., and Severinghaus, J.: Mean global ocean
639 temperatures during the last glacial transition. *Nature*, 553(7686), 39–44.
640 <https://doi.org/10.1038/nature25152>, 2018.
- 641 8. Bethke, I., Li, C., and Nisancioglu, K. H.: Can we use ice sheet reconstructions to constrain meltwater
642 for deglacial simulations? *Paleoceanography*, 27 (November 2011), 1–17.
643 doi:10.1029/2011PA002258, 2012
- 644 9. Böhm, E., Lippold, J., Gutjahr, M., Frank, M., Blaser, P., Antz, B., Fohlmeister, J., Frank, N.,
645 Andersen, M. B. and Deininger, M.: Strong and deep Atlantic meridional overturning circulation
646 during the last glacial cycle. *Nature*, 517(7534), 73–76. <https://doi.org/10.1038/nature14059>, 2015.
- 647 10. Bouttes, N., Roche, D. M., and Paillard, D.: Systematic study of the impact of fresh water fluxes on
648 the glacial carbon cycle, *Clim. Past*, 8, 589–607, <https://doi.org/10.5194/cp-8-589-2012>, 2012.
- 649 11. Bouttes, N., Lhardy, F., Quiquet, A., Paillard, D., Goosse, H., and Roche, D. M.: Deglacial climate
650 changes as forced by different ice sheet reconstructions, *Clim. Past*, 19, 1027–1042,
651 <https://doi.org/10.5194/cp-19-1027-2023>, 2023.
- 652 12. Buizert, C., Gkinis, V., Severinghaus, J. P., He, F., Lecavalier, B. S., Kindler, P., Leuenberger, M.,
653 Carlson, A. E., Vinther, B., Masson-Delmotte, V., White, J. W. C., Liu, Z., Otto-Bliesner, B., and
654 Brook, E. J.: Greenland temperature response to climate forcing during the last deglaciation, *Science*,
655 345, 1177–1180, [10.1126/science.1254961](https://doi.org/10.1126/science.1254961), 2014.
- 656 13. Buizert, C., Fudge, T. J., Roberts, W. H., Steig, E. J., Sherriff-Tadano, S., Ritz, C., Lefebvre, E.,
657 Edwards, J., Kawamura, K., Oyabu, I., Motoyama, H. Kahle, E. C., Jones, T. R., Abe-ouchi, A.,
658 Obase, T., Martin, C., Corr, H., Severinghaus, J. P., Beaudette, R. Epifanio, J. A., Brook, E. J., Martin,
659 K., Aoki, S., Nakazawa, T., Sowers, T. A., Alley, R. B., Ahn, J., Sigl, M., Severi, M., Dunbar, N. W.,
660 Svensson, A., Fegyveresi, J. M., He, C., Liu, Z., Zhu, J., Otto-bliesner, B. L., Lipenkov, V. Y.,
661 Kageyama, M., and Schwander, J.: Antarctic surface temperature and elevation during the Last
662 Glacial Maximum, *Science* 372(6546), 1097-1101, doi: 10.1126/science.abd2897, 2021
- 663 14. Burke, A. and Robinson, L. F.: The Southern Ocean’s Role in Carbon Exchange During the Last
664 Deglaciation, *Science*, 135, 6068, 557-561. <https://doi.org/10.1126/science.1208163>, 2011



- 665 15. Capron, E., Landais, A., Chappellaz, J., Schilt, A., Buiron, D., Dahl-Jensen, D., Johnsen, S. J., Jouzel,
666 J., Lemieux-Dudon, B., Loulergue, L., Leuenberger, M., Masson-Delmotte, V., Meyer, H., Oerter,
667 H., and Stenni, B.: Millennial and sub-millennial scale climatic variations recorded in polar ice cores
668 over the last glacial period, *Clim. Past*, 6, 345–365, <https://doi.org/10.5194/cp-6-345-2010>, 2010.
- 669 16. Chan, W.-L. and Abe-Ouchi, A.: Pliocene Model Intercomparison Project (PliMIP2) simulations
670 using the Model for Interdisciplinary Research on Climate (MIROC4m), *Clim. Past*, 16, 1523–1545,
671 <https://doi.org/10.5194/cp-16-1523-2020>, 2020.
- 672 17. Clark, P. U., He, F., Golledge, N. R., Mitrovica, J. X., Dutton, A., Hoffman, J. S., and Dendy,
673 S.: Oceanic forcing of penultimate deglacial and last interglacial sea-level rise. *Nature*, 577(7792),
674 660–664. <https://doi.org/10.1038/s41586-020-1931-7>, 2020
- 675 18. Condron, A., & Winsor, P.: Meltwater routing and the Younger Dryas. *Proceedings of the National*
676 *Academy of Sciences*, 109(49), 19928–19933, <https://doi.org/10.1073/pnas.1207381109>, 2012
- 677 19. Crosta, X., Kohfeld, K. E., Bostock, H. C., Chadwick, M., Du Vivier, A., Esper, O., Etourneau, J.,
678 Jones, J., Leventer, A., Müller, J., Rhodes, R. H., Allen, C. S., Ghadi, P., Lamping, N., Lange, C. B.,
679 Lawler, K.-A., Lund, D., Marzocchi, A., Meissner, K. J., Menviel, L., Nair, A., Patterson, M., Pike,
680 J., Prebble, J. G., Riesselman, C., Sadatzki, H., Sime, L. C., Shukla, S. K., Thöle, L., Vorrath, M.-E.,
681 Xiao, W., and Yang, J.: Antarctic sea ice over the past 130 000 years – Part 1: a review of what proxy
682 records tell us, *Clim. Past*, 18, 1729–1756, <https://doi.org/10.5194/cp-18-1729-2022>, 2022.
- 683 20. Dansgaard, W., Johnsen, S. J., Clausen, H. B., Dahl-Jensen, D., Gundestrup, N. S., Hammer, C. U.,
684 Hvidberg, C. S., Steffensen, J. P., Sveinbjörnsdottir, A. E., Jouzel, J., and Bond, G.: Evidence for
685 general instability of past climate from a 250-kyr ice-core record, *Nature*, 364, 218–220,
686 <https://doi.org/10.1038/364218a0>, 1993
- 687 21. Deschamps, P., Durand, N., Bard, E., Hamelin, B., Camoin, G., Thomas, A. L., Henderson, G. M.,
688 Okuno, J., and Yokoyama, Y.: Ice-sheet collapse and sea-level rise at the Bølling warming 14,600
689 years ago, *Nature*, 28, 559–564, <https://doi.org/10.1038/nature10902>, 2012.
- 690 22. Golledge, N., Menviel, L., Carter, L., Fogwill, C. J., England, M. H., Cortese, G., and Levy, R. H.:
691 Antarctic contribution to meltwater pulse 1A from reduced Southern Ocean overturning. *Nat*
692 *Commun* 5, 5107, <https://doi.org/10.1038/ncomms6107>, 2014.



- 693 23. Gomez, N., Weber, M. E., Clark, P. U., Mitrovica, J. X. and Han, H. K.: Antarctic ice dynamics
694 amplified by Northern Hemisphere sea-level forcing, *Nature*, 587(7835), 600–604,
695 doi:10.1038/s41586-020-2916-2, 2020
- 696 24. Gottschalk, J., Battaglia, G., Fischer, H., Frölicher, T. L., Jaccard, S. L., Jeltsch-Thömmes, A., Joos,
697 F., Köhler, P., Meissner, K. J., Menviel, L., Nehrbass-Ahles, C., Schmitt, J., Schmittner, A., Skinner,
698 L. C., and Stocker, T. F.: Mechanisms of millennial-scale atmospheric CO₂ change in numerical
699 model simulations, *Quaternary Sci. Rev.*, 220, 30–74,
700 <https://doi.org/10.1016/j.quascirev.2019.05.013>, 2019.
- 701 25. Gray, W. R., de Lavergne, C., Willis, R. C. J., Menviel, L., Spence, P., Holzer, M., Kageyama, M.
702 and Michel, E.: Poleward Shift in the Southern Hemisphere Westerly Winds Synchronous With the
703 Deglacial Rise in CO₂, *Paleoceanography and Paleoclimatology*, 38, 7,
704 <https://doi.org/10.1029/2023PA004666>, 2023
- 705 26. Green, R. A., Menviel, L., Meissner, K. J., Crosta, X., Chandan, D., Lohmann, G., Peltier, W. R., Shi,
706 X., and Zhu, J.: Evaluating seasonal sea-ice cover over the Southern Ocean at the Last Glacial
707 Maximum, *Clim. Past*, 18, 845–862, <https://doi.org/10.5194/cp-18-845-2022>, 2022.
- 708 27. Gregoire, L. J., Payne, A. J., and Valdes, P. J.: Deglacial rapid sea level rises caused by ice-sheet
709 saddle collapses, *Nature*, 487, 219–222, 10.1038/nature11257, 2012.
- 710 28. He, C., Zhengyu Liu, and Aixue Hu.: The transient response of atmospheric and oceanic heat
711 transports to anthropogenic warming. *Nature Climate Change*, 1, doi:10.1038/s41558-018-0387-3,
712 2019.
- 713 29. He, C., Liu, Z., Otto-Bliesner, B. L., Brady, E. C., Zhu, C., Tomas, R., Bao, Y.: Hydroclimate
714 footprint of pan-Asian monsoon water isotope during the last deglaciation. *Science Advances*, 7(4),
715 1–12. <https://doi.org/10.1126/sciadv.abe2611>, 2021.
- 716 30. Hunter, S. J., Haywood, A. M., Dolan, A. M., and Tindall, J. C.: The HadCM3 contribution to
717 Pliocene phase 2, *Clim. Past*, 15, 1691–1713, <https://doi.org/10.5194/cp-15-1691-2019>, 2019.
- 718 31. Ivanovic, R. F., Gregoire, L. J., Kageyama, M., Roche, D. M., Valdes, P. J., Burke, A., Drummond,
719 R., Peltier, W. R., and Tarasov, L.: Transient climate simulations of the deglaciation 21–9 thousand



- 720 years before present (version 1) – PMIP4 Core experiment design and boundary conditions, *Geosci.*
721 *Model Dev.*, 9, 2563–2587, <https://doi.org/10.5194/gmd-9-2563-2016>, 2016.
- 722 32. Ivanovic, R. F., Gregoire, L. J., Burke, A., Wickert, A. D., and Valdes, P. J.: Acceleration of Northern
723 Ice Sheet Melt Induces AMOC Slowdown and Northern Cooling in Simulations of the Early Last
724 Deglaciation, *Paleoceanography and Paleoclimatology*. 807–824. doi:10.1029/2017PA003308, 2018
- 725 33. Jouzel, J., Masson-Delmotte, V., Cattani, O., Dreyfus, G., Falourd, S., Hoffmann, G., Minster, B.,
726 Nouet, J., Barnola, J. M., Chappellaz, J., Fischer, H., Gallet, J. C., Johnsen, S., Leuen-
727 berguer, M., Loulergue, L., Luethi, D., Oerter, H., Parrenin, F., Raisbeck, G., Raynaud, D., Schilt, A., Schwander,
728 J., Selmo, E., Souchez, R., Spahni, R., Stauffer, B., Steffensen, J. P., Stenni, B., Stocker, T. F., Tison,
729 J. L., Werner, M., and Wolff, E. W.: Orbital and Millennial Antarctic Climate Variability over the
730 Past 800,000 Years, *Science*, 317, 793-796, <https://doi.org/10.1126/science.1141038>, 2007.
- 731 34. Kageyama, M., Merkel, U., Otto-Bliesner, B., Prange, M., Abe-Ouchi, A., Lohmann, G., Ohgaito,
732 R., Roche, D. M., Singarayer, J., Swingedouw, D., and X Zhang: Climatic impacts of fresh water
733 hosing under Last Glacial Maximum conditions: a multi-model study, *Clim. Past*, 9, 935–953,
734 <https://doi.org/10.5194/cp-9-935-2013>, 2013.
- 735 35. Kageyama, M., Braconnot, P., Harrison, S. P., Haywood, A. M., Jungclaus, J. H., Otto-Bliesner, B.
736 L., Peterschmitt, J.-Y., Abe-Ouchi, A., Albani, S., Bartlein, P. J., Brierley, C., Crucifix, M., Dolan,
737 A., Fernandez-Donado, L., Fischer, H., Hopcroft, P. O., Ivanovic, R. F., Lambert, F., Lunt, D. J.,
738 Mahowald, N. M., Peltier, W. R., Phipps, S. J., Roche, D. M., Schmidt, G. A., Tarasov, L., Valdes,
739 P. J., Zhang, Q., and Zhou, T.: The PMIP4 contribution to CMIP6 – Part 1: Overview and over-
740 arching analysis plan, *Geosci. Model Dev.*, 11, 1033–1057, [https://doi.org/10.5194/gmd-11-1033-](https://doi.org/10.5194/gmd-11-1033-2018)
741 [2018](https://doi.org/10.5194/gmd-11-1033-2018), 2018.
- 742 36. Kageyama, M., Harrison, S. P., Kapsch, M.-L., Lofverstrom, M., Lora, J. M., Mikolajewicz, U.,
743 Sherriff-Tadano, S., Vadsaria, T., Abe-Ouchi, A., Bouttes, N., Chandan, D., Gregoire, L. J., Ivanovic,
744 R. F., Izumi, K., LeGrande, A. N., Lhardy, F., Lohmann, G., Morozova, P. A., Ohgaito, R., Paul, A.,
745 Peltier, W. R., Poulsen, C. J., Quiquet, A., Roche, D. M., Shi, X., Tierney, J. E., Valdes, P. J., Volodin,
746 E., and Zhu, J.: The PMIP4 Last Glacial Maximum experiments: preliminary results and comparison



- 747 with the PMIP3 simulations, *Clim. Past*, 17, 1065–1089, <https://doi.org/10.5194/cp-17-1065-2021>,
748 2021.
- 749 37. Kapsch, M.-L., Mikolajewicz, U., Ziemen, F. and Schannwell, C.: Ocean response in transient
750 simulations of the last deglaciation dominated by underlying ice-sheet reconstruction and method of
751 meltwater distribution, *Geophysical Research Letters*, 49, e2021GL096767,
752 <https://doi.org/10.1029/2021GL096767>, 2022.
- 753 38. Kuniyoshi, Y., Abe-Ouchi, A., Sherriff-Tadano, S., Chan, W.-L., and Saito, F.: Effect of Climatic
754 Precession on Dansgaard-Oeschger-Like Oscillations. *Geophysical Research Letters*, 49(6),
755 e2021GL095695. <https://doi.org/10.1029/2021GL095695>, 2022.
- 756 39. Kobayashi, H., Oka, A., Yamamoto, A., and Abe-Ouchi, A.: Glacial carbon cycle changes by
757 Southern Ocean processes with sedimentary amplification. *Science Advances*, 7(35), doi:
758 10.1126/sciadv.abg7723, 2021.
- 759 40. Lambeck, K., Rouby, H., Purcell, A., Sun, Y., and Sambridge, M.: Sea level and global ice volumes
760 from the Last Glacial Maximum to the Holocene, *P. Natl. Acad. Sci.*, 111, 15296–15303,
761 10.1073/pnas.1411762111, 2014.
- 762 41. Lhardy, F., Bouttes, N., Roche, D. M., Crosta, X., Waelbroeck, C., and Paillard, D.: Impact of
763 Southern Ocean surface conditions on deep ocean circulation during the LGM: a model analysis,
764 *Clim. Past*, 17, 1139–1159, <https://doi.org/10.5194/cp-17-1139-2021>, 2021.
- 765 42. Lisiecki, L. E. and Raymo, M. E.: A Pliocene-Pleistocene stack of 57 globally distributed benthic
766 $\delta^{18}\text{O}$ records, *Paleoceanography*, 20, PA1003, doi:10.1029/2004PA001071, 2005
- 767 43. Liu, Z., Otto-Bliesner, B. L., He, F., Brady, E. C., Tomas, R., Clark, P. U., Carlson, A. E., Lynch-
768 Stieglitz, J., Curry, W., Brook, E., Erickson, D., Jacob, R., Kutzbach, J., and Cheng, J.: Transient
769 Simulation of Last Deglaciation with a New Mechanism for Bølling-Allerød Warming, *Science*, 325,
770 310–314, 10.1126/science.1171041, 2009
- 771 44. Lowry, D. P., Golledge, N. R., Menviel, L., and Bertler, N. A. N.: Deglacial evolution of regional
772 Antarctic climate and Southern Ocean conditions in transient climate simulations. 189–215, 2018.



- 773 45. Lynch-Stieglitz, J., Adkins, J. F., Curry, W. B., Dokken, T., Hall, I. R., Herguera, J. C. and Zahn, R.:
774 Atlantic meridional overturning circulation during the Last Glacial Maximum. *Science*, 316(5821),
775 66–69. <https://doi.org/10.1126/science.1137127>, 2007
- 776 46. MacDougall, A. H., Frölicher, T. L., Jones, C. D., Rogelj, J., Matthews, H. D., Zickfeld, K., Arora,
777 V. K., Barrett, N. J., Brovkin, V., Burger, F. A., Eby, M., Eliseev, A. V., Hajima, T., Holden, P. B.,
778 Jeltsch-Thömmes, A., Koven, C., Mengis, N., Menviel, L., Michou, M., Mokhov, I. I., Oka, A.,
779 Schwinger, J., Séférian, R., Shaffer, G., Sokolov, A., Tachiiri, K., Tjiputra, J., Wiltshire, A., and
780 Ziehn, T.: Is there warming in the pipeline? A multi-model analysis of the Zero Emissions
781 Commitment from CO₂, *Biogeosciences*, 17, 2987–3016, <https://doi.org/10.5194/bg-17-2987-2020>,
782 2020.
- 783 47. Marcott, S. A., Bauska, T. K., Buizert, C., Steig, E. J., Rosen, J. L., Cuffey, K. M., Fudge, T. J.,
784 Severinghaus, J. P., Kalk, M. L., McConnell, J. R., Sowers, T., Taylor, K. C. White, J. W. C. and
785 Brook, E. J.: Centennial-scale changes in the global carbon cycle during the last deglaciation. *Nature*,
786 514(7524), 616–619. <https://doi.org/10.1038/nature13799>, 2014
- 787 48. Margari, V., Skinner, L. C., Menviel, L., Capron, E., Rhodes, R. H., Martrat, B., and Grimalt, J. O.:
788 Fast and slow components of interstadial warming in the North Atlantic during the last glacial.
789 *Communications Earth & Environment*, 1–9. <https://doi.org/10.1038/s43247-020-0006-x>, 2020
- 790 49. Mariotti, V., Paillard, D., Bopp, L., Roche, D. M., and Bouttes, N.: A coupled model for carbon and
791 radiocarbon evolution during the last deglaciation. *Geophysical Research Letters*, 43(3), 1306–1313.
792 <https://doi.org/10.1002/2015GL067489>, 2016.
- 793 50. Marson, J. M., Mysak, L. A., Mata, M. M., and Wainer, I.: Evolution of the deep Atlantic water
794 masses since the last glacial maximum based on a transient run of NCAR-CCSM3. *Climate Dynamics*,
795 47(3–4), 865–877. <https://doi.org/10.1007/s00382-015-2876-7>, 2016
- 796 51. Martínez-García, A., Rosell-Melé, A., Jaccard, S.: Southern Ocean dust–climate coupling over the
797 past four million years. *Nature* 476, 312–315. <https://doi.org/10.1038/nature10310>, 2011.
- 798 52. Martrat, B., Grimalt, J. O., Shackleton, N. J., de Abreu, L., Hutterli, M.A., and Stocker, T. F.: Four
799 climate cycles of recurring deep and surface water destabilizations on the Iberian Margin, *Science*,
800 317, 502–507, doi:10.1126/science.1139994, 2007.



- 801 53. Marzocchi, A. and Jansen, M. F. Global cooling linked to increased glacial carbon storage via
802 changes in Antarctic sea ice. *Nature Geoscience*, 12, 1001–1005, [https://doi.org/10.1038/s41561-](https://doi.org/10.1038/s41561-019-0466-8)
803 019-0466-8, 2019
- 804 54. McManus, J. F., Francois, R., Gherardi, J.-M., Keigwin, L. D., and Brown-Leger, S.: Collapse and
805 rapid resumption of Atlantic meridional circulation linked to deglacial climate changes, *Nature*, 428,
806 834–837, [10.1038/nature02494](https://doi.org/10.1038/nature02494), 2004.
- 807 55. Menviel, L., Yu, J., Joos, F., Mouchet, A., Meissner, K. J., and England, M. H.: Poorly ventilated
808 deep ocean at the Last Glacial Maximum inferred from carbon isotopes: A data-model comparison
809 study. *Paleoceanography*, 32(1), 2–17. <https://doi.org/10.1002/2016PA003024>, 2017.
- 810 56. Menviel, L., Timmermann, a., Timm, O. E., and Mouchet, A.: Climate and biogeochemical response
811 to a rapid melting of the West Antarctic Ice sheet during interglacials and implications for future
812 climate. *Paleoceanography*, 25, 1–12. <https://doi.org/10.1029/2009PA001892>, 2010.
- 813 57. Menviel, L., Timmermann, A., Timm, O. E., and Mouchet, A.: Deconstructing the Last Glacial
814 termination: the role of millennial and orbital-scale forcings, *Quaternary Sci. Rev.*, 30, 1155–1172,
815 [10.1016/j.quascirev.2011.02.005](https://doi.org/10.1016/j.quascirev.2011.02.005), 2011.
- 816 58. Menviel, L., England, M. H., Meissner, K. J., Mouchet, A., and Yu, J.: Atlantic-Pacific seesaw and
817 its role in outgassing CO₂ during Heinrich events. *Paleoceanography*, 29(January), 58–70.
818 <https://doi.org/10.1002/2013PA002542>, 2014.
- 819 59. Menviel, L., Spence, P., Yu, J., Chamberlain, M. A., Matear, R. J., Meissner, K. J., and England, M.
820 H.: Southern Hemisphere westerlies as a driver of the early deglacial atmospheric CO₂ rise. *Nature*
821 *Communications*, 9(1), 1–12. <https://doi.org/10.1038/s41467-018-04876-4>, 2018
- 822 60. Moros, M., De Deckker, P., Perner, K., Ninnemann, U. S., Wacker, L., Telford, R., Jansen, E., Blanz,
823 T. and Schneider, R.: Hydrographic shifts south of Australia over the last deglaciation and possible
824 interhemispheric linkages. *Quaternary Research (United States)*, 102, 130–141.
825 <https://doi.org/10.1017/qua.2021.12>, 2021
- 826 61. Moy, A. D., Palmer, M. R., Howard, W. R., Bijma, J., Cooper, M. J., Calvo, E., Pelejero, C., Gagan,
827 M. K. and Chalk, T. B.: Varied contribution of the Southern Ocean to deglacial atmospheric CO₂
828 rise. *Nature Geoscience*, 12(12), 1006–1011. <https://doi.org/10.1038/s41561-019-0473-9>, 2019



- 829 62. Ng, H. C., Robinson, L. F., McManus, J. F., Mohamed, K. J., Jacobel, A. W., Ivanovic, R. F.,
830 Gregoire, L. J. and Chen, T.: Coherent deglacial changes in western Atlantic Ocean circulation.
831 Nature Communications, 9(1), 1–10. <https://doi.org/10.1038/s41467-018-05312-3>, 2018
- 832 63. Obase, T., and Abe- Ouchi, A.: Abrupt Bølling-Allerød warming simulated under gradual forcing of
833 the last deglaciation, Geophysical Research Letters, 46, <https://doi.org/10.1029/2019GL084675>,
834 2019.
- 835 64. Obase, T., A. Abe-Ouchi, F. Saito: Abrupt climate changes in the last two deglaciations simulated
836 with different Northern ice sheet discharge and insolation, Scientific Reports, 11, doi:
837 10.1038/s41598-021-01651-2, 2021
- 838 65. Parrenin, F., Masson-Delmotte, V., Köhler, P., Raynaud, D., Paillard, D., Schwander, J., Barbante,
839 C., Landais, A., Wegner, A., Jouzel, J.: Atmospheric carbon dioxide, methane, deuterium, and
840 calculated Antarctic temperature of EPICA Dome C ice core. PANGAEA,
841 doi:10.1594/PANGAEA.810199, 2013
- 842 66. Pedro, J. B., Martin, T., Steig, E. J., Jochum, M., Park, W., & Rasmussen, S. O.: Southern Ocean
843 deep convection as a driver of Antarctic warming events. Geophysical Research Letters, 43(5), 2192–
844 2199. <https://doi.org/10.1002/2016GL067861>, 2016
- 845 67. Pedro, J. B., Jochum, M., Buizert, C., He, F., Barker, S., & Rasmussen, S. O.: Beyond the bipolar
846 seesaw: Toward a process understanding of interhemispheric coupling. Quaternary Science Reviews,
847 192, 27–46. <https://doi.org/10.1016/j.quascirev.2018.05.005>, 2018
- 848 68. Peltier, W. R., Argus, D. F., and Drummond, R.: Space geodesy constrains ice age terminal
849 deglaciation: The global ICE-6G_C (VM5a) model, J. Geophys. Res.-Sol. Ea., 120, 450–487,
850 10.1002/2014JB011176, 2015.
- 851 69. Petit, J. R., Jouzel, J., Raynaud, D., Barkov, N. I., Barnola, J.-M., Basile, I., Bender, M., Chappellaz,
852 J., Davis, M., Delaygue, G., Delmotte, M., Kotlyakov, V. M., Legrand, M., Lipenkov, V. Y., Lorius,
853 C., PÉpin, L., Ritz, C., Saltzman, E., and Stievenard, M.: Climate and atmospheric history of the past
854 420 000 years from the Vostok ice core, Antarctica, Nature, 399, 429–436, 10.1038/20859, 1999.



- 855 70. Pöppelmeier, F., Jeltsch-Thömmes, A., Lippold, J. et al. Multi-proxy constraints on Atlantic
856 circulation dynamics since the last ice age. *Nat. Geosci.* 16, 349–356 (2023).
857 <https://doi.org/10.1038/s41561-023-01140-3>
- 858 71. Rae, J. W. B., Burke, A., Robinson, L. F., Adkins, J. F., Chen, T., Cole, C., Greenop, R., Li, T.,
859 Littley, E. F. M., Nita, D. C., Stewart, J. A. and Taylor, B. J.: CO₂ storage and release in the deep
860 Southern Ocean on millennial to centennial timescales, *Nature*, 562, 569–573,
861 <https://doi.org/10.1038/s41586-018-0614-0>, 2018
- 862 72. Renssen, H., Mairesse, A., Goosse, H., Mathiot, P., Heiri, O., Roche, D. M., Nisancioglu, K. H. and
863 Valdes, P. J.: Multiple causes of the Younger Dryas cold period. *Nature Geoscience*, 8(12), 946–949.
864 <https://doi.org/10.1038/ngeo2557>, 2015
- 865 73. Roberts, N. L., Piotrowski, A. M., McManus, J. F., and Keigwin, L. D.: Synchronous Deglacial
866 Overturning and Water Mass Source Changes, *Science*, 327, 75–78, 10.1126/science.1178068, 2010.
- 867 74. Roche, D. M., Renssen, H., Paillard, D., & Levavasseur, G.: Deciphering the spatio-temporal
868 complexity of climate change of the last deglaciation: A model analysis. *Climate of the Past*, 7(2),
869 591–602. <https://doi.org/10.5194/cp-7-591-2011>, 2011
- 870 75. Rojas, M., Moreno, P., Kageyama, M., Crucifix, M., Hewitt, C., Abe-Ouchi, A., Ohgaito, R., Brady
871 E. C. and Hope, P.: The Southern Westerlies during the last glacial maximum in PMIP2 simulations.
872 *Climate Dynamics*, 32(4), 525–548. <https://doi.org/10.1007/s00382-008-0421-7>, 2009
- 873 76. Seroussi, H., Nowicki, S., Payne, A. J., Goelzer, H., Lipscomb, W. H., Abe-Ouchi, A., Agosta, C.,
874 Albrecht, T., Asay-Davis, X., Barthel, A., Calov, R., Cullather, R., Dumas, C., Galton-Fenzi, B. K.,
875 Gladstone, R., Golledge, N. R., Gregory, J. M., Greve, R., Hattermann, T., Hoffman, M. J., Humbert,
876 A., Huybrechts, P., Jourdain, N. C., Kleiner, T., Larour, E., Leguy, G. R., Lowry, D. P., Little, C. M.,
877 Morlighem, M., Pattyn, F., Pelle, T., Price, S. F., Quiquet, A., Reese, R., Schlegel, N.-J., Shepherd,
878 A., Simon, E., Smith, R. S., Straneo, F., Sun, S., Trusel, L. D., Van Breedam, J., van de Wal, R. S.
879 W., Winkelmann, R., Zhao, C., Zhang, T., and Zwinger, T.: ISMIP6 Antarctica: a multi-model
880 ensemble of the Antarctic ice sheet evolution over the 21st century, *The Cryosphere*, 14, 3033–3070,
881 <https://doi.org/10.5194/tc-14-3033-2020>, 2020.



- 882 77. Severinghaus, J. P. and Brook, E. J.: Abrupt Climate Change at the End of the Last Glacial Period
883 Inferred from Trapped Air in Polar Ice, *Science*, 286, 930–934, [10.1126/science.286.5441.930](https://doi.org/10.1126/science.286.5441.930), 1999.
- 884 78. Shakun, J. D., Clark, P. U., He, F., Marcott, S. A., Mix, A. C., Liu, Z., Otto-Bliesner, B., Schmittner,
885 A., and Bard, E.: Global warming preceded by increasing carbon dioxide concentrations during the
886 last deglaciation, *Nature*, 484, 49–54, [10.1038/nature10915](https://doi.org/10.1038/nature10915), 2012.
- 887 79. Sherriff-Tadano, S., Abe-Ouchi, A., Yoshimori, M., Ohgaito, R., Vadsaria, T., Chan, W-L., Hotta,
888 H., Kikuchi, M., Kodama, T., Oka, A., Southern Ocean surface temperatures and cloud biases in
889 climate models connected to the representation of glacial deep ocean circulation, *Journal of Climate*.
890 3849-3866, <https://doi.org/10.1175/JCLI-D-22-0221.1>, 2023
- 891 80. Sigman, D. M., Hain, M. P., & Haug, G. H.: The polar ocean and glacial cycles in atmospheric CO₂
892 concentration. *Nature*, 466(7302), 47–55. <https://doi.org/10.1038/nature09149>, 2010
- 893 81. Sikes, E. L., Schiraldi, B., & Williams, A.: Seasonal and Latitudinal Response of New Zealand Sea
894 Surface Temperature to Warming Climate Since the Last Glaciation: Comparing Alkenones to
895 Mg/Ca Foraminiferal Reconstructions. *Paleoceanography and Paleoclimatology*, 34(11), 1816–1832.
896 <https://doi.org/10.1029/2019PA003649>, 2019.
- 897 82. Sime, L. C., Kohfeld, K. E., Le, C., Wolff, E. W., Boer, A. M. De, Graham, R. M., & Bopp, L.:
898 Southern Hemisphere westerly wind changes during the Last Glacial Maximum: model-data
899 comparison. *Quaternary Science Reviews*, 64, 104–120.
900 <https://doi.org/10.1016/j.quascirev.2012.12.008>, 2013.
- 901 83. Skinner, L. C., Fallon, S., Waelbroeck, C., Michel, E., & Barker, S.: Ventilation of the deep Southern
902 Ocean and deglacial CO₂ rise. *Science*, 328(5982), 1147–1151.
903 <https://doi.org/10.1126/science.1183627>, 2010
- 904 84. Snoll, B., Ivanovic, R.F., Valdes, P.J., Maycock, A. C. and Gregoire, L. J.: Effect of orographic
905 gravity wave drag on Northern Hemisphere climate in transient simulations of the last deglaciation.
906 *Clim Dyn* 59, 2067–2079. <https://doi.org/10.1007/s00382-022-06196-2>, 2022.
- 907 85. Steffensen, J. P., Andersen, K. K., Bigler, M., Clausen, H. B., Dahl-Jensen, D., Fischer, H., Goto-
908 Azuma, K., Hansson, M., Johnsen, S. J., Jouzel, J., Masson-Delmotte, V., Popp, T., Rasmussen, S.
909 O., Röthlisberger, R., Ruth, U., Stauffer, B., Siggaard-Andersen, M.-L., Sveinbjörnsdóttir, Á. E.,



- 910 Svensson, A., and White, J. W. C.: High-Resolution Greenland Ice Core Data Show Abrupt Climate
911 Change Happens in Few Years, *Science*, 321, 680–684, 10.1126/science.1157707, 2008.
- 912 86. Stein, K., Timmermann, A., Young Kwon, E., and Friedrich, T.: Timing and magnitude of Southern
913 Ocean sea ice/carbon cycle feedbacks, *P. Natl. Acad. Sci. USA*, 117, 9,
914 <https://doi.org/10.1073/pnas.1908670117>, 2020.
- 915 87. Stocker, T. F., & Johnsen, S. J.: A minimum thermodynamic model for the bipolar seesaw.
916 *Paleoceanography*, 18(4), 1–9. <https://doi.org/10.1029/2003PA000920>, 2003
- 917 88. Stouffer, R. J., Yin, J., Gregory, J. M., Dixon, K. W., & Spelman, M. J.: Investigating the Causes of
918 the Response of the Thermohaline Circulation to Past and. *Journal of Climate*, 19, 1365–1387.
919 <https://doi.org/10.1002/9781119115397.ch25>, 2006
- 920 89. Tarasov, L., Dyke, A. S., Neal, R. M., and Peltier, W. R.: A data-calibrated distribution of deglacial
921 chronologies for the North American ice complex from glaciological modeling, *Earth Planet. Sci.*
922 *Lett.*, 315–316, 30–40, 10.1016/j.epsl.2011.09.010, 2012
- 923 90. Tierney, J. E., Zhu, J., King, J., Malevich, S. B., Hakim, G. J., & Poulsen, C. J.: Glacial cooling and
924 climate sensitivity revisited. *Nature*, 584(7822), 569–573. [https://doi.org/10.1038/s41586-020-2617-](https://doi.org/10.1038/s41586-020-2617-x)
925 *x*, 2020
- 926 91. Timmermann, A., Timm, O., Stott, L., and Menviel, L.: The roles of CO₂ and orbital forcing in
927 driving Southern Hemispheric temperature variations during the last 21 000 Yr. *Journal of Climate*,
928 22(7), 1626–1640. <https://doi.org/10.1175/2008JCLI2161.1>, 2009
- 929 92. Toucanne, S., Zaragosi, S., Bourillet, J.-F., Marieu, V., Cremer, M., Kageyama, M., Van Vliet-Lanoë,
930 B., Eynaud, F., Turon, J.-L., and Gibbard, P.-L.: The first estimation of Fleuve Manche palaeoriver
931 discharge during the last deglaciation: Evidence for Fennoscandian ice sheet meltwater flow in the
932 English Channel ca 20–18 ka ago, *Earth Planet. Sc. Lett.*, 290, 459–473, 2010.
- 933 93. WAIS Divide Project Members: Onset of deglacial warming in West Antarctica driven by local
934 orbital forcing. *Nature*, 500(7463), 440–444. <https://doi.org/10.1038/nature12376>, 2013.
- 935 94. WAIS Divide project members: Precise inter polar phasing of abrupt climate change during the last
936 ice age. *Nature*, 520(7549), 661–665. <https://doi.org/10.1038/nature14401>, 2015



- 937 95. Yoshimori, M., Yokohata, T., and Abe-Ouchi, A.: A Comparison of Climate Feedback Strength
938 between CO₂ Doubling and LGM Experiments, *J. Climate*, 22, 3374–3395,
939 <https://doi.org/10.1175/2009JCLI2801.1>, 2009.
- 940 96. Zhu, J. and Poulsen, C. J.: Last Glacial Maximum (LGM) climate forcing and ocean dynamical
941 feedback and their implications for estimating climate sensitivity, *Clim. Past*, 17, 253–267,
942 <https://doi.org/10.5194/cp-17-253-2021>, 2021.
- 943
- 944